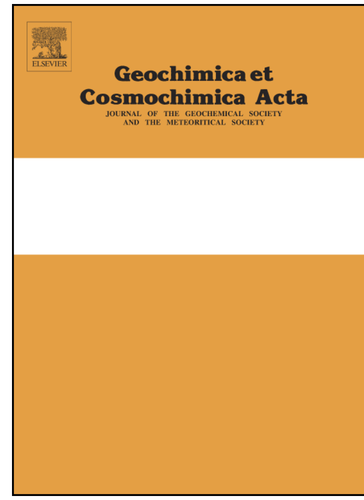

Geochemistry and Age of Shatsky, Hess, and Ojin Rise seamounts: Implications for a connection between the Shatsky and Hess Rises

Maria Luisa G. Tejada, Jörg Geldmacher, Folkmar Hauff, Daniel Heaton, Anthony A.P. Koppers, Dieter Garbe-Schönberg, Kaj Hoernle, Ken Heydolph, William W. Sager

PII: S0016-7037(16)30165-X
DOI: http://dx.doi.org/10.1016/j.gca.2016.04.006
Reference: GCA 9701

To appear in: *Geochimica et Cosmochimica Acta*

Received Date: 4 September 2015
Accepted Date: 1 April 2016

Geochemistry and Age of Shatsky, Hess, and Ojin Rise seamounts: Implications for a connection between the Shatsky and Hess Rises

Maria Luisa G. Tejada [a,b]*, Jörg Geldmacher [c], Folkmar Hauff [c], Daniel Heaton [d], Anthony A. P. Koppers [d], Dieter Garbe-Schönberg [e], Kaj Hoernle [c, e], Ken Heydolph [c], and William W. Sager[f]

[a] Department of Solid Earth Geochemistry, Japan Agency for Marine-Earth Science and Technology, 2-15 Natsushima, Yokosuka, 237-0061 Japan mtejada@jamstec.go.jp
[b] Research and Development Center for Submarine Resources, Japan Agency for Marine-Earth Science and Technology, 2-15 Natsushima, Yokosuka, 237-0061 Japan
[c] GEOMAR, Helmholtz-Zentrum für Ozeanforschung Kiel, Wischhofstr. 1-3, D-24148 Kiel, Germany
[d] College of Earth, Ocean and Atmospheric Sciences, Oregon State University, Corvallis, Oregon, 97331 USA
[e] Institute of Geosciences, University of Kiel, Germany
[f] Department of Earth and Atmospheric Sciences, University of Houston, Houston, TX 77204 USA

*corresponding author

Submitted to

Geochimica et Cosmochimica Acta Special Issue in honor of Fred Frey

Abstract

Shatsky Rise in the Northwest Pacific is the best example so far of an oceanic plateau with two potential hotspot tracks emanating from it: the linear Papanin volcanic ridge and the seamounts comprising Ojin Rise. Arguably, these hotspot tracks also project toward the direction of Hess Rise, located ~1200 km away, leading to speculations that the two plateaus are connected. Dredging was conducted on the massifs and seamounts around Shatsky Rise in an effort to understand the relationship between these plateaus and associated seamounts. Here, we present new $^{40}Ar/^{39}Ar$ ages and trace element and Nd, Pb, and Hf isotopic data for the recovered dredged rocks and new trace elements and isotopic data for a few drill core samples from Hess Rise. Chemically, the samples can be subdivided into plateau basalt-like tholeiites and trachytic to alkalic ocean-island basalt compositions, indicating at least two types of volcanic activity. Tholeiites from the northern Hess Rise (DSDP Site 464) and the trachytes from Toronto Ridge on Shatsky's TAMU massif have isotopic compositions that overlap with those of the drilled Shatsky Rise plateau basalts, suggesting that both Rises formed from the same mantle source. In contrast, trachytes from the southern Hess Rise (DSDP Site 465A) have more radiogenic Pb isotopic ratios that are shifted toward a high time-integrated U/Pb (HIMU-type mantle) composition. The compositions of the dredged seamount samples show two trends relative to Shatsky Rise data: one toward lower $^{143}Nd/^{144}Nd$ but similar $^{206}Pb/^{204}Pb$ ratios, the other toward similar $^{143}Nd/^{144}Nd$ but more radiogenic $^{206}Pb/^{204}Pb$ ratios. These trends can be attributed to lower degrees of melting either from lower mantle material during hotspot-related transition to plume tail or from less refractory shallow mantle components tapped during intermittent deformation-related volcanism induced by local tectonic extension between and after the

main volcanic-edifice building episodes on Shatsky Rise. The ocean-island-basalt-like chemistry and isotopic composition of the Shatsky and Hess rise seamounts contrast with those formed by purely deformation-related shallow mantle-derived volcanism, favoring the role of a long-lived mantle anomaly in their origin. Finally, new $^{40}Ar/^{39}Ar$ evidence indicates that Shatsky Rise edifices may have been formed in multiple-stages and over a longer duration than previously believed.

1. Introduction

One of the outstanding problems with a plume origin model for many oceanic plateaus is the absence of a link to a post-plateau, time-progressive hotspot track. This is especially true for the Ontong Java Plateau (OJP), the largest oceanic plateau on Earth. However, Shatsky Rise in the Northwest Pacific Ocean is the best Pacific example of an oceanic plateau with two potential hotspot tracks emanating from it: the relatively continuous North Flank-Papanin ridge and the seamounts trail comprising Ojin Rise (Fig. 1; Sager etal., 1999). Shatsky Rise is a massive oceanic plateau, covering an area of $4.8x10^5$ km^2 similar to the size of California (Sager et al., 1999; Sager, 2005) and consists of three discrete volcanic edifices (Fig. 1a): the TAMU Massif, the ORI Massif, and the Shirshov Massif (Sager et al., 1999), that become younger (Geldmacher et al., 2014; Heaton & Koppers, 2014) and smaller in volume toward the northeast (Sager et al., 1999), consistent with the southwestward trajectory of the Pacific plate's motion from 145-125 Ma (Larson et al., 1992; Kroenke, 1996; Sager, 2007; Sager et al., 2015). The northeast flank of the Shirshov Massif is truncated by a WNW-trending graben. Across this graben, Shatsky Rise continues with the prominent NE-SW oriented Papanin Ridge, which extends to 43^oN where it bends eastward, towards the Hess Rise, a similar large, neighboring oceanic plateau (Fig. 1b). Immediately east of the Shirshov Massif sprawl the Ojin Rise Seamounts, capping a broad, discontinuous, ESE-trending swell (Fig. 1; Sager etal., 1999; Nakanishi et al., 1999).

Previous geophysical studies attribute the origin of Shatsky Rise to the interplay of a mantle plume from the lower mantle with a spreading center triple junction (Sager and Han, 1993; Nakanishi et al., 1989; 1999) but whether or not the melting anomaly continued on to the Hess Rise, via North Flank-Papanin Ridge or via the Ojin Rise is still speculative. The decreasing size from TAMU to Shirshov, which tapers into the North Flank and Papanin Ridge, has been suggested to reflect a waning magmatic activity of the mantle plume that produced the Shatsky Rise (Sager et al., 1999; Sager, 2005). On the other hand, the Ojin Rise seamounts emanating from Shirshov could be construed as hotspot track representing the "plume head to tail" stage of hotspot development (Sager et al., 1999; Nakanishi et al., 1999). Hess Rise could potentially link to one of these two possible hotspot tracks (Fig. 1b), leading to speculations that it could represent a second large magmatic outpouring of the melting anomaly that formed Shatsky Rise about 30-35 my earlier.

Seismic and bathymetric data also reveal the presence of subsidiary volcanic cones around and on the Shatsky Rise massifs (Sager et al., 1999; Sager et al., 2013; Zhang et al., 2015). Some of these cones appear to disturb Cretaceous sediments deposited on the plateau, suggesting that the cones post-date formation of the plateau basement. The data also reveal a profusion of seamounts to the north and east of the Shirshov Massif and the presence of northeast-southwest-trending seamounts cutting across the rise between the TAMU Massif in the south and ORI and Shirshov massifs to the north. One example is Cooperation Seamount, located between the ORI Massif and TAMU Massif (indicated by dredge haul D11 on Fig. 1a). Whether or not these and similar features are also part of the primary volcanism that formed Shatsky Rise is unknown. This study is an initial step toward understanding the origin and potential relationship of the Shatsky Rise and Hess Rise to the seamounts associated with them.

We conducted trace element and Nd-Hf-Pb isotopic studies and $^{40}Ar/^{39}Ar$ dating of volcanic rocks recovered by dredging during the Cruise TN037 of the *R/V Thomas G. Thompson* in 1994 (Sager et al., 1995; 1999; Table 1; Fig. 1). This cruise recovered basalts from two of the seamounts on Shatsky Rise [Cooperation Seamount in the Helios Basin between Tamu and Ori Massifs (D11), Earthwatch Seamount on the North Flank of Shatsky Rise (D4)] and two Ojin Rise Seamounts [Victoria Seamount (D2) and Seamount 6 (D1)]. Samples were also recovered from the eastern summit of ORI Massif (D9) and the Toronto Ridge on TAMU Massif (D13 and D14). The isotopic compositions of two dredged samples from ORI and TAMU have been reported previously (Mahoney et al., 2005) but their ages are reported here for the first time. New Nd-Hf-Pb isotopic and trace element data are also reported for Deep-Sea Drilling Project (DSDP) Sites 464 and 465A samples from Hess Rise, complementing the sparse available geochemical dataset for these neighboring oceanic plateaus (Mahoney, 1987; Mahoney et al., 2005). The main goal is to elucidate the relationship, if any, of the dredged seamounts to Shatsky Rise and whether or not they represent post-plateau magmatic activity of the proposed plume head that formed the rise.

Our results confirm that the tholeiitic basalts from the northern part of Hess Rise have similar isotopic compositions to the plateau basalts from the main Shastky Rise massifs, consistent with double flood basalt event model for the two rises. In addition, both rises seem to progress from older tholeiitic and isotopically depleted to younger alkalic and isotopically more enriched volcanism. The transition from plateau to ocean island type volcanism could be explained by a) decreasing degree of melting with declining temperature or increasing depth of melting, or both; b) preferential sampling of enriched components in a heterogeneous source as the degree of melting declines; and c) sampling of totally different mantle sources. Our data show that the isotopic range displayed by the seamounts maybe explained either by low-degree melting of enriched components in the underlying (post-plateau) upper mantle caused by small voluminous decompression melting at local extension zones or by melting from isotopically distinct lower mantle material in the Shatsky-Hess plume mantle.

2. Sample locations, petrography and major element characteristics

Locations of dredge hauls conducted on seamounts (and selected for this study) are shown in Fig. 1 and listed in Table 1. Dredges D1 and D2 were conducted on Ojin Rise Seamounts: D1 was on Seamount 6 near the eastern end of the rise close to the Emperor Seamount Chain, whereas D2 was on Seamount 8 (Victoria Seamount), one of several seamounts located to the east of the Shatsky Rise's Shirshov Massif. Igneous rocks recovered in D1 are massive, amygdaloidal to glomeroporphyritic pillow fragments. They are highly altered, with varying degrees of oxidation and chloritization of the groundmass, typical of submarine alteration. Ferromanganese encrustation and dendrites are common in most specimens, though less abundant in some. Some rocks have well-defined alteration rinds with less-altered interiors. Fragments for isotopic and chemical analysis were taken from the visibly least altered parts of such samples. A few small fragments of highly to moderately altered massive aphyric lava from the cores of ferromanganese nodules were recovered from D2. The volcanic cores are green-gray, mottled with brown-gray discoloration, and contain rare vesicles (~1 mm) filled with clay, ferromanganese oxide, carbonate, or a mixture of the three.

Dredge haul D4 was conducted on Earthwatch Seamount on the North Flank of Shatsky Rise (between Shirshov and Papanin Ridge) and D11 on Cooperation Seamount (between the Tamu and Ori Massifs) (Fig. 1; Table 1). The recovered samples consist of basaltic to trachytic volcanic rocks that are finely vesicular and aphyric to sparsely plagioclase-phyric. These rocks contrast with the massive, dense, holocrystalline rocks consisting of plagioclase $\pm$ clinopyroxene $\pm$ olivine (altered to iddingsite) and the coarsely vesicular, dense, aphyric rocks from D9 on ORI massif, but are similar to the massive but less dense plagioclase-phyric samples from D13 and D14 from the Toronto Ridge on the TAMU massif (Sager et al., 1995).

Major element compositions of the recovered dredged samples from cruise TN037 suggest a bimodal grouping (Fig. 2; data from Tatsumi et al., 1998). One group with MgO >4 wt%, consisting mostly of plateau samples from the ORI Massif (Mahoney et al., 2005) and a sample from Earthwatch Seamount shows a range of basaltic compositions similar to the drilled Shatsky Rise tholeiites (Sano et al., 2012). The other group with MgO <4 wt%, from the Earthwatch Seamount, Ojin Rise Seamounts, Cooperation Seamount, Toronto Ridge, including a few vesicular dredge samples from the ORI Massif, have compositions that range from trachyandesite to trachyte. Petrographic analysis (Appendix A) revealed that these samples contain only plagioclase and trace amounts of mafic minerals as phenocrysts, indicating that their low MgO is likely to be a magmatic feature. The high TiO_2 contents of the Ojin Rise Seamounts (2.1-3.0 wt%), Earthwatch Seamount (2.0-4.6 wt%), Cooperation Seamount (2.0-2.6 wt%), and some Toronto Ridge samples (1.8-2.4 wt% for D13-01 and D13-02) could likewise indicate that their high Na_2O and K_2O contents may partly reflect a transitional to alkalic nature (Tatsumi et al., 1998). Furthermore, their higher Nb and Zr contents compared to mid-ocean ridge basalts (MORB) and Shatsky Rise tholeiites plotting within the Iceland Array in Zr/Y-Nb/Y plot, suggest transitional to ocean island basalts affinity (Fig. 3).

Bimodal lithologies were also cored at Hess Rise during DSDP Leg 62 (Fig. 2; Vallier et al., 1980; 1983; Seifert et al., 1981; Windom et al., 1981). Samples for this study were selected from igneous rocks recovered at Sites 464 and 465A (see Thiede et al., 1981 and Vallier et al., 1983). Sixteen centimeters of tholeiitic basalt was encountered below lower Albian to upper Aptian (~113 Ma) sediments at the base of the hole at Site 464, located at the deep, elongated northwesterly extension of Hess Rise probably representing older parts of the plateau (Seifert et al., 1981; Vallier et al., 1983). In contrast, 24 m of trachyte, interpreted as subaerial lava flows, were cored below late Albian-early Cenomanian (~100-95 Ma) sediments at Site 465A located at the high crest near the steep southern edge of the plateau (Thiede et al., 1981; Scott, 1981). Attempts to determine the radiometric ages of the Site 465 drill samples failed but yielded minimum ages of 90-94 Ma consistent with overlying sediment ages (Pringle and Dalrymple, 1993).

3. Analytical methods

Based on macroscopic observations, the least altered-appearing rock fragments from each dredge were selected for trace element and isotopic study. Among those selected, the least altered interior portions of the freshest-looking rocks were reserved for isotopic analysis. Bulk-sample major elements and Rb, Ba, Nb, Sr, Zr, Y, and Ni abundances were determined by X-ray fluorescence spectrometry (Figs. 2 and 3) on slabs or fragments of the same rock used for isotope analysis and were reported by Tatsumi et al. (1998). Major element and isotope ratio measurements were not always possible on the same rock sample because of sample size limitations. However, samples analyzed for bulk trace element measurements were from the same piece of rock measured for isotopes, except for D2-01, where this was not possible because of the small size of the rock fragment recovered.

Trace element analyses for seamount samples (Table 2) were conducted at Japan Agency for Marine-Earth Science and Technology (JAMSTEC) laboratory by inductively-coupled-plasma spectrometry (ICP-MS) using an Agilent 7500ce (Chang et al., 2002). Trace element concentrations for the drilled Hess Rise DSDP samples were also determined by ICP-MS at the Institute of Geoscience at University of Kiel (IGUK) using an AGILENT 7500cs following the methods outlined in Garbe-Schönberg (1993). Sample preparation details are described in Appendix B. Analytical precision as estimated from both duplicate digestions and replicate analyses was better than 1-2% RSD for all elements. Accuracy is estimated based on international rock standards that were digested and analyzed as unknowns together with the samples (Table 2). The results of these measurements, such as for BHVO-2, processed both at JAMSTEC and at IGUK, agree very well within ≤1% (for Rb, Th, U, Nb, Ta, La, Ce, Pr, Nd, Eu, Dy, Ho, Lu, Co, and Cu) and ≤6% (Sr, Zr, Gd, Tb, Y, Er, Tm, Yb, Sc, Ni) of each other except for Ta, Hf and Pb with 8%, 11%, and 24% differences, respectively.

Isotope ratio measurements for Nd and Pb were conducted on 0.2-0.4 cm chips that were acid-cleaned and handpicked under the microscrope at both University of Hawaii (UH) and GEOMAR isotope laboratories (see notes in Table 3 and Appendix B for sample preparation details for each laboratory). A subset of seamount (TN037-D1-12, TN037-D2-01, TN037-D4-13, TN037-D11-01) and Hess Rise (464-34R-CC and 465-42R-2, 76-78) samples were analyzed for Nd and Pb isotopes at UH following the procedures reported previously for dredged Shatsky Rise samples (Mahoney et al., 2005). For these samples, the concentrations of Sm, Nd, Pb, U, and Th were determined by isotope dilution on the same sample solutions used for isotope ratio measurements (Table 3). Hafnium isotope analyses were carried out on splits of the same set of samples, and Nd, Pb, and Hf isotopes were also measured on additional seamount samples and Hess Rise DSDP drill core samples, at GEOMAR. Analytical procedures are as previously described for drilled Shatsky Rise samples (Heydolph et al., 2014) and are summarized in Appendix B. Sample preparation and cleaning procedures vary but the Nd and Pb isotope results are in excellent agreement, as demonstrated for the drilled Hess Rise samples analyzed in both laboratories (Table 3).

Six samples were chosen to be most suitable for argon geochronology analysis, consisting of variably altered trachytes from Toronto Ridge and Cooperation Seamounts and a tholeiite from ORI Massif (Table 4). Samples that were prepared for plagioclase analysis were required to have abundant minimally altered plagioclase phenocrysts. Groundmass samples were chosen based on their high crystallinity and significant regions of minimally altered microphenocrysts and mesostasis. Three groundmass (TN037-D11 and TN037-D9), and three fresh (TN037-D13) to minimally altered plagioclase (TN037-D14), samples were analyzed. The samples were prepared using the methods of Koppers et al. (2011) and are described in Appendix A.

4. Results

4.1 $^{40}Ar/^{39}Ar$ ages

The incremental heating technique was used to slowly degas grains in order to remove alteration typically present in the lower temperature steps (e.g. Koppers et al., 2000; 2004). All argon ages were measured relative to the flux monitor standard FCT-NM sanidine

(28.201 ± 0.082 Ma, 1σ; Kuiper et al. 2008) and calculated using the corrected Steiger and Jager (1977) decay constant of 5.530 ± 0.097 x 10^{-10} 1/yr (2σ) as reported by Min et al. (2000). In total, 23-44 heating steps were applied for groundmass samples and, for plagioclase, 19-24 steps were used (Table 4; Fig. 4). Groundmass samples displayed discordant ages with the incremental heating patterns revealing significant argon recoil (TN037 D11-01) or both argon recoil and argon loss (TN037 D11-05; TN037 D9-04). Both groundmass samples also show relatively high K/Ca at lower temperatures indicating substantial hydrothermal and seawater alteration. Even though the groundmass samples do not provide reliable plateau ages, sample D11-05 exhibits a pseudo plateau (19% ^{39}Ar) at ~122 Ma that is supported by a concordant inverse isochrons age (Figure 4 inset) and an ^{40}Ar/^{36}Ar intercept of 295 ± 12 that is within the atmospheric value of 295.5. Since TN037 D11-05 also displays argon loss, this would be considered a minimum age. In a similar way, sample TN037 D9-04 gives a minimum age estimate of ~117 Ma for the ORI Massif.

Plagioclase separates were prepared on samples from Toronto Ridge only (Fig. 4). TN037 D13-02 contained 95% of the ^{39}Ar gas in the plateau with an MSWD of 0.80 and provides a confident eruption age for lavas making up Toronto Ridge at 129.42 ± 0.32 Ma, the same as the earlier reported age of 128.2 ± 0.5 Ma (Heaton and Koppers, 2014) but corrected using FCT-NM (28.201 Ma, Kuiper et al., 2008). The other two plagioclase analyses displayed argon loss and some minor excess argon at the higher temperature steps. TN037 D14-01A and TN037 D14-01B are from the same rock, whereby D14-01B is visibly more altered in hand sample than D14-01A, which is reflected in the higher K/Ca ratio patterns (Fig. 4) observed during the incremental heating experiments. TN037 D14-01A also displays a pseudo plateau reflecting a minimum age of ~121 Ma and contains excess argon in the higher temperature steps, which is evident in the inverse isochrons diagram of this sample as well.

In summary, the results provide a confident eruption age for the trachytes that comprise Toronto Ridge at 129.4 ± 0.3 Ma, but the other groundmass dating results only provide minimum ages due to severe alteration of the samples and presence of excess argon. However, some insight into the ages of the seamounts may be gleaned from those discordant analyses, indicating that Cooperation seamount erupted at ≥122 Ma and the late-stage East ORI Massif summit sometime at ≥117 Ma.

4.2 Trace element characteristics and alteration assessment

A potential problem of any geochemical study on old submarine samples is the effect of seawater alteration and concomitant precipitation of secondary authigenic minerals, especially in highly to moderately vesicular samples. The intimate association of ferromanganese encrustation and phosphorization has been observed by, for example, Hein et al. (1993) in equatorial Pacific seamounts and is known to occur on seamounts elsewhere (Cullen and Burnett, 1986; Jarvis et al., 1994; Wheat et al., 1996). Thus, only samples that do not show anomalously high Fe_2O_3* and MnO and coupled high (≥5 wt%) P_2O_5 and CaO (Tatsumi et al., 1998; Tejada, 1998), indicative of ferromanganese contamination and phosphorization, were included in this study (Figs. 2-3). Note that for similar moderately to highly phosphorized dredged rocks from an OJP seamount, Hanyu et al. (2015a) showed that samples with P_2O_5 below 5 wt% still preserve magmatic trace elements and isotope compositions.

Chondrite-normalized rare-earth element (REE) patterns also suggest that most of the samples included in this study were not significantly affected by incorporation of phosphates and ferromanganese oxide materials. Both phosphorization and ferromanganese contamination could lead to elevated REE except Ce and possibly Eu because of their lower relative contents in these materials (Fig. 5). Accordingly, samples (e.g., TN037-D1-10, TN037-D4-01) that show elevated REE coupled with apparently strong negative anomalies in Ce and Eu, were not considered for isotope ratio determination (Fig. 5; Table 3). Note that most of the Cooperation Seamount samples display coherent rare earth element patterns with no negative Ce anomalies, similar to the drillcore samples from Site 465 on Hess Rise (Fig. 5), suggesting their generally fresher nature compared to most Ojin Rise and Earthwatch seamounts samples. On the other hand, several samples from both Ojin and North Flank Earthwatch seamount show only very little (D1-05, D1-08, D4-05, D4-13) to minor (D1-12, D4-12) signs of relict (possibly microscopic) incorporation of Fe-oxides or phosphates not completely removed by picking and acid cleaning. These samples, together with the Cooperation Seamount samples, were therefore used for isotopic ratio measurements.

Considering only samples that display the least altered trace element compositions, the Earthwatch (North Flank, D4) and Ojin Rise (D1) samples show almost identical characteristics that contrast clearly with those of Cooperation Seamount (D11) (Fig. 6). All of the seamounts have enriched mantle compositions distinct from MORB in Zr/Y-Nb/Y discrimination plot (Fig. 3). Both Earthwatch and Ojin Rise samples have relatively flat rare-earth element patterns [$(Ce/Yb)_n$= 1.02-1.87 and 1.82-2.90, respectively] and only mildly enriched multi-element primitive mantle-normalized incompatible trace element signatures with slightly depleted HREE (more pronounced for Ojin Rise seamount trachytes) and no clear Nb-Ta anomaly (Fig. 6). Although the Ojin and Earthwatch seamount samples possess higher absolute trace element concentrations, their multi-element patterns are identical or very similar (except for elevated Rb, and U) to Shatsky's Normal type lavas such as found on Shirshov Massif, the youngest Shatsky massif (Heydolph et al., 2014), and OJP tholeiites (Tejada et al., 2002), respectively. The Ojin Rise trachytes share the steeper slope in heavy rare earth element and slightly humped-back shape of the Shirshov pattern relative to those of the OJP tholeiites but with higher $(Sm/Yb)_n$ (≥ 2) (Figs. 3, 5-6). On the other hand, the trace element patterns of the Earthwatch seamount samples are almost parallel with those of the OJP basalts (neglecting the positive spikes in Rb, U, and La, which are indicative of relict alteration) and have similar $(Nb/Yb)_n$, $(Ce/Yb)_n$, and $(Sm/Yb)_n$ to TAMU and Shirshov basalts (Fig. 3). Their chondrite-normalized rare earth element patterns are also elevated, with a sloping trend in light rare earth elements relative to those of DSDP Site 464 Hess Rise tholeiites, as shown by this and prior studies (Figs. 3 and 5; Seifert et al., 1981; Vallier et al., 1983).

In contrast, Cooperation Seamount samples show strongly enriched primitive-mantle-normalized incompatible trace element and REE patterns $(Sm/Yb)_n$= 3.1-3.4) similar to alkalic ocean island basalts or to late stage alkalic rocks dredged from the Manihiki (e.g., D3, Ingle et al., 2007; Hoernle et al., 2008; 2009) and Hikurangi (Hoernle et al., 2005; 2010) plateaus, which are considered part of the Greater Ontong Java plateau event (Taylor, 2006; Davy et al., 2008; Hoernle et al., 2008, 2009, 2010; Timm et al., 2011). Their chondrite-normalized rare earth element patterns run parallel and their absolute concentrations are also very similar to the Hess Rise alkalic trachytes from DSDP Site 465A (Fig. 5; Table 2;

Seifert et al., 1981; Scott, 1981). Furthermore, their trace element abundances are almost overlapping (Fig. 6) with those of the Sigana alkalic basalt samples associated with the OJP tholeiites (Tejada et al., 1996), except for Rb, Nb, and Sr.

4.3 Nd-Hf-Pb isotopes

The very similar trace element and REE patterns observed for the least altered samples from each seamount indicate that they could be part of similar or the same respective eruptive flows on each seamount. This is also shown in the measured (present-day) Nd-Hf and Pb isotopic compositions of samples from each of the different seamounts (Appendix B and Tables B.1 and B.2). As outlined in Appendix B, we prefer to use the isotope dilution-derived parent-daughter ratios measured at UH for similar samples (based on identical or similar trace element patterns) from each location to estimate the age-correction on measured Nd and Pb isotopic ratios analyzed at GEOMAR (Table 3, Figs. 7 and 8).

Because of the more altered nature of some of the present samples compared with those used in our previous works, we have used a strong leaching technique (e.g., Mahoney, 1987; Mahoney and Spencer 1991), which was also adopted by Nobre-Silva et al. (2009; 2010), during the earlier part of the study (Appendix B; Tejada, 1998; Tejada et al., 2001). Strong leaching recovers near magmatic isotope values but also affect Sm, Nd, and Th concentrations in more altered rocks, which leads to elevated age-corrected Nd isotope ratios (e.g., Thompson et al., 2008) and $^{208}Pb/^{204}Pb$ values as reported by Huang et al. (2005). Based on our own previous works and experience (e.g., Tejada, 1998; Hoernle et al., 2010;

Heydolph et al., 2014), as well as the results from the few strongly leached samples, we found that for old and moderately altered rocks, weak leaching on chips before digestion and determination of parent-daughter ratios on the same sample solution used for isotopic ratio measurements is the best compromise to derive the original near-magmatic Nd and Pb isotopic composition. For this reason, we used the isotope-dilution-derived parent-daughter abundances from powder splits made from acid-cleaned (weakly leached) chips for age-correction of all the isotope data within the same magmatic suite of rocks (Table 3, Appendix B). This method is tantamount to applying an average age-correction for each magmatic suite based on representative samples for each group and results in convergence in the isotopic data for strongly- and weakly- leached samples for each seamount and less scatter in isotope plots (Table 3, Figs. 7-8; Appendix B).

4.3.1 Toronto Ridge and ORI Massif, Shatsky Rise (129 Ma)

Isotopic data for Sr, Nd, and Pb for Toronto Ridge on Shatsky Rise were reported previously (Mahoney et al., 2005) but are age-adjusted here (using standard radiogenic growth equations) to the new eruption age of 129 Ma. The age-corrected isotopic compositions, are $\varepsilon_{Nd}(t)$ = +9.9, $(^{206}Pb/^{204}Pb)_t$=18.17, $(^{207}Pb/^{204}Pb)_t$=15.45, and $(^{208}Pb/^{204}Pb)_t$=37.74, which plot well within the isotopic field of the drilled Shatsky Rise basement and overlap or plot very close to those of TAMU Massif basement with $\varepsilon_{Nd}(t)$ = +9.0 to +10.5, $(^{206}Pb/^{204}Pb)_t$=18.151-18.464, $(^{207}Pb/^{204}Pb)_t$=15.453-14.471, and $(^{208}Pb/^{204}Pb)_t$=37.718-37.970 (Heydolph et al., 2014). Compared to ORI massif dredge sample D9-01B (Mahoney et al., 2005), the Toronto Ridge trachyte possesses slightly higher $\varepsilon_{Nd}(t)$, $(^{206}Pb/^{204}Pb)_t$ and lower $(^{207}Pb/^{204}Pb)_t$ (Figs. 7-8).

4.3.2 Hess Rise (>110 Ma)

The initial isotopic compositions for Hess Rise (using 110 Ma for age correction) show two distinct signatures, indicating a significant systematic difference between the sources of the two DSDP sites 464 and 465A lavas. Site 464 tholeiites yield relatively depleted isotopic compositions, with $(^{206}Pb/^{204}Pb)_t$= 18.15-18.29, $(^{207}Pb/^{204}Pb)_t$= 15.48-15.50, and $(^{208}Pb/^{204}Pb)_t$= 37.86-37.96, $\varepsilon_{Nd}(t)$ = +8.3 to +8.9, and $\varepsilon_{Hf}(t)$ = +14.5 plotting within the data ranges reported for the Shatsky Rise plateau in all isotope plots (Figs. 7-8). In particular, the Site 464 Hess Rise data plot close to those of the ORI dredge sample, TN037-D9-01B (Mahoney et al., 2005) and both have isotopic compositions that are within the range of normal type basalt from ORI Massif drill Site U1350, with $(^{206}Pb/^{204}Pb)_t$= 18.068-18.645, $(^{207}Pb/^{204}Pb)_t$= 15.437-15.473, and $(^{208}Pb/^{204}Pb)_t$= 37.616-38.103, $\varepsilon_{Nd}(t)$ = +8.7 to +10.0, and $\varepsilon_{Hf}(t)$ = 10.4 to +15.0 (Heydolph et al., 2014), except for the slightly higher $(^{207}Pb/^{204}Pb)_t$.

In contrast, Site 465A trachytes are isotopically much more enriched than Site 464 tholeiites, with $(^{206}Pb/^{204}Pb)_t$= 19.00-19.07, $(^{207}Pb/^{204}Pb)_t$= 15.59-15.60, and $(^{208}Pb/^{204}Pb)_t$= 39.24-39.41, $\varepsilon_{Nd}(t)$ = +5.5 to +6.1, and $\varepsilon_{Hf}(t)$ = +6.8 and plot close to the data fields for dredged Manihiki tholeiites and Hikurangi alkalic basalts (Mahoney and Spencer, 1991; Hoernle et al., 2005; 2010; Timm et al., 2011) except for their higher $(^{208}Pb/^{204}Pb)_t$ ratios (Figs. 7-8). These isotopic compositions also plot close or within the compositional fields for Samoan shield basalts in all isotope plots. The low $\varepsilon_{Hf}(t)$ and high $(^{206}Pb/^{204}Pb)_t$ of Site 465A trachytes indicate more affinity with HIMU-type basalts from Hikurangi and Manihiki plateaus (Hoernle et al., 2005; 2010). For reference, other alkalic rocks from Manihiki plateaus, as well as the alkalic rock associated with the OJP, also have age-corrected $^{206}Pb/^{204}Pb$ ratios of greater than 19 (Hoernle et al., 2010; Tejada et al., 1996). The isotopic contrast with those of Site 464 tholeiites is much greater than can be expected from possible effects of crystallization with attendant assimilation of oceanic lithosphere (presumably with MORB-like isotopic compositions) to form the Site 465A trachytes from alkalic basalts with the same source as the Hess Rise tholeiites.

4.3.3 Ojin Rise, Earthwatch, and Cooperation seamounts (>120 Ma)

The samples from the Ojin Rise seamounts also show a range of isotopic compositions with distinct differences between the easternmost and westernmost seamounts (Figs. 7-8). Sample D2-01 from Victoria Seamount, closest to Shatsky's Shirshov Massif, has $\varepsilon_{Nd}(t)$ = +7.0, $(^{206}Pb/^{204}Pb)_t$=18.32, $(^{207}Pb/^{204}Pb)_t$=15.54, and $(^{208}Pb/^{204}Pb)_t$=38.18. These values are relatively closer to Shatsky Rise than to the Ojin Rise Seamount 6 compositions, especially in Pb-Pb diagrams. The data points plot consistently near the OJP fields in $\varepsilon_{Nd}(t)$ vs. $(^{206}Pb/^{204}Pb)_t$ and all Pb-Pb isotope diagrams. Trachytes from Seamount 6 have $\varepsilon_{Nd}(t)$ = +6.8 to +10.1, $\varepsilon_{Hf}(t)$ = +9.3 to +10.0, $(^{206}Pb/^{204}Pb)_t$=18.65-18.87, $(^{207}Pb/^{204}Pb)_t$=15.55-15.58, and $(^{208}Pb/^{204}Pb)_t$=38.65-38.86, values that are transitional between those of the isotopically more depleted (predominantly tholeiitic) Shatsky lavas and the more radiogenic Hess Rise Site 465 trachytes and dredged Manihiki and Hikurangi alkalic rocks. These isotopic compositions also plot close to those of the older (80-65 Ma) Louisville alkalic basalts (Cheng et al., 1987; Beier et al., 2011; Vanderkluysen et al., 2014; Williams et al., 2014) that show affinity to a focal zone mantle (FOZO; Hart et al., 1992) inferred to represent a common component in the source of some ocean island basalts and in both Manihiki and Hikurangi plateaus (Hoernle et al., 2010; Timm et al., 2011).

Like Victoria Seamount, Earthwatch Seamount data, from the northern flank of Shatsky Rise, have isotopic compositions of $\varepsilon_{Nd}(t)$ = +4.9 to +5.4, $\varepsilon_{Hf}(t)$ = +8.2 to +9.7, $(^{206}Pb/^{204}Pb)_t$=17.95-18.17, $(^{207}Pb/^{204}Pb)_t$=15.55-15.56, and $(^{208}Pb/^{204}Pb)_t$=37.99-38.14] that plot close or within the data fields for Ontong Java and Hikurangi plateau basalts, except for slightly higher $(^{207}Pb/^{204}Pb)_t$ (Figs. 7-8). Although the lower initial Pb isotope ratios of these samples compared to Ojin Rise trachytes could be an artifact of a possible over-correction due to alteration-modified higher parent-daughter ratios, the Pb isotopic composition is consistent with their (more alteration-resistant) $\varepsilon_{Nd}(t)$ and $\varepsilon_{Hf}(t)$ values that are also more OJP-like (Fig. 7). Their isotopic compositions are also consistent with their lower $(Sm/Yb)_n$, $(Nb/Yb)_n$ and (Ce/Yb)n compared to Ojin Rise seamounts and with their trace element patterns that are more OJP-like, except for being shifted to higher abundances (Figs. 3 and 6).

In contrast, the Pb isotopic compositions of samples from the Cooperation Seamount, despite its location at the center of Shatsky Rise, differ markedly from those of the plateau basalts and Toronto Ridge and are shifted toward the more radiogenic Pb isotopic compositions of the Ojin Rise Seamount 6 trachytes (Figs. 7-8). Compared to the Seamount 6 data, however, these samples display a smaller range of isotopic compositions, with $(^{208}Pb/^{204}Pb)_t$= 38.72-39.02, $\varepsilon_{Nd}(t)$ = +7.3 to +8.7, higher $(^{206}Pb/^{204}Pb)_t$= 19.04-19.09 and $\varepsilon_{Hf}(t)$ = +11.6 to +11.7 and lower $(^{207}Pb/^{204}Pb)_t$= 15.54-15.55 for a given $(^{206}Pb/^{204}Pb)_t$. This composition is more akin to the Jurassic alkalic basalts overlying Jurassic MORB at ODP Site 801 (Castillo et al., 1992; Hauff et al., 2003) except for their higher $\varepsilon_{Hf}(t)$ and $(^{208}Pb/^{204}Pb)_t$. The data also plot close or within those of dredged Manihiki tholeiites and Louisville alkalic rocks.

5. Discussion

5.1 A Shatsky-Hess connection?

Several lines of geophysical and geochemical evidence suggest a hotspot origin for Shatsky Rise (Sager, 2005; Heydolph et al. 2014). These include the sheer volume and thickness of its oldest edifice, TAMU Massif, designated as the single largest volcano on Earth (Sager et al., 2013) and associated high eruption rate of 1.7 km^3/y estimated for this volcanic edifice (Sager and Han, 1993), which is comparable to that of Deccan and North Atlantic Tertiary Province flood volcanism (e.g., Richards et al., 1989; Coffin and Eldholm, 1994). Furthermore, the greater estimated depth of melting and higher degree of melting compared to MORB (Sano et al., 2012; Husen et al, 2013; Kimura and Kawabata, 2015) and the isotopic composition of several Shatsky basalts (Heydolph et al., 2014, Hanyu et al., 2015b), combined with the composition of Shirshov basalts plotting within the Iceland Array in Zr/Y-Nb/Y plot (Fig. 3), suggest a magma source distinct from the MORB source. A corollary of the plume initiation model is the prediction of a post-plateau hotspot track of seamounts, as trace of the "plume tail" that can be linked to a plateau. From Mesozoic plate-boundary reconstructions, Nakanishi et al. (1989; 1999) concluded that the Shatsky Rise hotspot formed the Papanin Ridge up to M5 time (128 Ma), after which it diminished in activity, disappearing entirely for a time shortly after the plate motion direction changed. This general picture is corroborated by paleolatitude measurements derived from nearby seafloor, indicating a southward motion of the Pacific plate prior to a change to northward motion after about 125 Ma (Larson et al., 1992; Sager, 2007). The change in plate motion is evident in the bend or "hook" of the Papanin Ridge at about 43^{o}N (Fig. 1), which has been suggested to imply a link between Shatsky Rise and Hess Rise (Pringle and Dalrymple, 1993; Kroenke and Sager, 1993; Bercovici and Mahoney, 1994; Sager et al., 1999; Nakanishi et al., 1999). Some workers suggest the possibility for the presence of two hotspot tracks in the vicinity of Shatsky Rise (e.g., Nakanishi et al., 1999; Sager et al., 1999) via the Papanin Ridge and/or the Ojin Rise Seamounts (solid and dashed arrows in Fig. 1b, respectively).

Given a possible link from Shatsky Rise to Hess Rise via either the 43°N Papanin Ridge bend or the Ojin Rise Seamounts, the two plateaus may have been formed from the same source. Hess Rise data cluster into two distinct isotopic groups, with the tholeiites from its northern branch, Site 464, overlapping the compositional fields for the tholeiitic Shatsky Rise plateau basalts in all four isotopic systems (Figs. 7 and 8). Although based only on one drill site and therefore to be treated with caution, this isotopic similarity provides strong support for the idea of a common source for both plateaus since the Hess Rise tholeiites do not show any other systematic and consistent compositional similarity with any other Pacific oceanic plateau or OIB compositional field in all four isotopic systems (Figs. 7, 8). Site 464 sits on seafloor formed during the Cretaceous Normal Superchron (CNS; 120.4-83.5 Ma, e.g., Chandler et al., 2015). The age difference of ~30-35 m.y. between the initiation of Shatsky plateau volcanism (145 Ma, Geldmacher et al., 2014; Heaton and Koppers 2014) and the minimum age of the Site 464 basement (≥110 Ma, Thiede et al., 1981) (Figs.1, 9; Table 1) based on biostratigraphic dating reflects a similar time lag between the two main volcanic pulses detected at Ontong Java (e.g., Mahoney et al., 1993; Tejada et al. 2002; Hoernle et al., 2010). Interestingly, tholeiitic lavas from the two volcanic episodes on OJP possess similar isotopic signatures (Mahoney et al., 1993; Tejada et al., 2002) analogous to those of Shatsky and Hess Rise tholeiites, although minor occurrences of alkalic dikes having HIMU-type compositions (Tejada et al., 1996; Hoernle et al., 2010) were also found. A model evolution of a Shatsky Rise mantle source that has previously undergone 15% melting in the garnet stability field (Sano et al., 2012) and isotopically evolved ~30-35 Ma thereafter shows isotopic signatures akin to that of Hess Rise mantle source at 110 Ma (Fig. 10), supporting a genetic link for the two rises. Age-correction of Hess Rise isotope composition to 145 Ma produced similar results.

Two (or even multiple) episodes of plateau volcanism also have been observed at other large igneous provinces such as the Broken Ridge-Kerguelen (Coffin et al., 2002) or Rio Grande Rise/Walvis Ridge-Parana/Etendeka (O'Connor and Duncan, 1990; Rohde et al. 2013) flood basalt pairs. Recent geophysical investigation also suggests multiple phases of magmatic activity on Manihiki Plateau (Pietsch and Uenzelmann-Neben, 2015). Proposed models for double or multiple plateau-forming events include separation or stalling of a starting mantle plume head while crossing the interface between upper and lower mantle (Bercovici and Mahoney, 1994; Fitton et al., 1997) and secondary instabilities during ascent (van Keken et al., 1997). The latter may be induced when the upwelling plume contains dense lithologies (Lin and van Keken, 2005) such as eclogite, which would be consistent with the presence of entrained recycled material as indicated by the isotopic composition of some Shatsky Rise lavas (Heydolph et al., 2014; Hanyu et al. 2015b). Alternatively, Hess Rise could represent a second LIP eruption formed by interaction of the same melting anomaly with another triple junction (Sager, 2005; Davies et al., 2015; O’Connor and Jokat, 2015).

5.2 Shatsky-seamounts connection?

The transition from plateau to seamount volcanism is often attributed to the waning magmatic activity because of declining temperature and depth of melting, resulting in lower degrees of melting of the same source with no significant change in isotopic composition of volcanic products with time. This is the case for the Toronto Ridge trachytes that retain identical isotopic compositions with the TAMU massif tholeiites (Figs. 7-8). The change in degree of magmatic output may also result in compositional change in volcanic products if the scale of heterogeneity in the mantle source is smaller than the degree of melting, resulting in preferential sampling of enriched material by low-degree melts. Alternatively, a compositional change in volcanic products would also result from sampling of totally different materials in a mixed or a zoned mantle source. The large contrast between Shatsky basalt composition and those of the seamounts suggests the latter two possibilities. None of the seamounts has compositions that can be consistently derived from Shatsky mantle source in all isotope plots but their individual estimated source composition constantly plot toward the more enriched lower bound composition of Shatsky Rise mantle source at 145 Ma, except for Pb isotopes (Fig. 10). Furthermore, the combined range of seamount isotopic composition overlaps with the range of the Shatsky Rise data in all isotope plots. The increase in the range of isotopic composition with time could suggest less homogenization of inherent plume heterogeneities caused by decreasing degree of melting (e.g., less dilution of enriched plume components by large melting volumes; Heydolph et al., 2014) or melting of axial zone material from the lower mantle (i.e., in a zoned plume mantle model). The second possibility is similar to a model proposed for Iceland, wherein a mantle plume originating from the lower mantle that stalls at 670 km discontinuity would contain mostly of heated upper mantle envelope that melts first, followed by entrained lower mantle material along its axial zone (Fitton et al., 1997). This model could also account for the MORB-like composition of the Shatsky Rise massifs and the more OIB-like signatures of the seamount trails associated with it.

5.2.1 Cooperation and Ojin Rise seamounts link to plateau volcanism?

The isotopic composition of Cooperation Seamount and the sampled Ojin Rise seamounts (D1) approach those of Louisville and some Samoan shield basalts (Figs. 7-8) inferred to represent a focal zone (FOZO; Hart et al., 1992) component, proposed to represent lower mantle material, which is also suggested as a main component in the Manihiki, Hikurangi, and possibly Ontong Java, plateau sources (Hoernle et al., 2010; Timm et al., 2011; Tejada et al., 2015a). Like the Ojin Rise and Cooperation seamounts, the numerous seamounts superimposed on the Manihiki and Hikurangi plateaus began to form about 20 m.y. after the plateau-forming event. The formation of late stage, low volume, alkalic volcanic structures seems to be a common phenomenon on many (if not most) oceanic plateaus, e.g., at Ontong Java, Manihiki, and Hikurangi plateaus (Beiersdorf et al., 1995; Tejada et al., 1996; 2015b; Ingle et al., 2007; Hoernle et al., 2008; 2009; 2010; Timm et al., 2011; Shimizu et al., 2015; Pietsch and Uenzelmann-Neben, 2015).

The transition to a more radiogenic Pb isotopic composition also coincidentally appears to accompany the second eruption phase in both Shatsky-Hess and OJP. For Hess Rise, this is evident from the trend of the southern Hess Rise Site 465 trachytes isotopic compositions [minimum age of ~95 Ma (Pringle and Dalrymple, 1993), ~10 million years younger than the northern Hess Rise Site 464 tholeiites] toward high integrated U/Pb (HIMU)-type isotope composition. Likewise, alkalic basalts from the 90 Ma Sigana eruptive event on the Ontong Java Plateau and from the 75-82 Ma Manihiki and 67-99 Ma Hikurangi seamounts also show a HIMU-type (characterized by radiogenic $^{206}Pb/^{204}Pb$ isotopic composition) affinity, indicating that such a component may have been also present in the greater Ontong Java mantle source (Tejada et al., 1996; Hoernle et al. 2005; 2010; Timm et al., 2011). HIMU-type mantle evidently was also involved in producing the older (157 Ma) ODP Site 801 alkalic lavas (Figs. 7 and 8) and the younger (~120 Ma) Cooperation Seamount and Marcus-Wake Seamounts to the south (Staudigel et al., 1991; Castillo et al., 1992; Konter et al., 2008; Shimoda et al., 2011), 10-25 m. y. before and after emplacement of the TAMU and ORI massifs. Thus, this HIMU-type mantle source seems to be present in a large and apparently long-lived thermally and isotopically anomalous region in the South Pacific (Staudigel et al., 1991), close to where the oceanic plateaus formed, and possibly represent plume mantle material in the Shatsky Rise source.

5.2.2 North Flank-Papanin link to plateau volcanism?

Papanin Ridge seems to be the clearest morphological link between Shatsky and Hess Rise (solid arrow in Fig. 1). Unfortunately, no samples are available from the Papanin Ridge. However, our data from the Earthwatch Seamount (D4) on the North Flank of the Shirshov Massif, adjacent to Papanin Ridge, imply the presence of an OJP-like mantle component (Figs. 7 and 8), suggested to represent near-primitive lower mantle material (Tejada et al., 2004; Jackson and Carlson, 2011) at the end of Shatsky plateau volcanism. It is also noteworthy that the sample from Victoria Seamount (D2) located closest to Shirshov Massif, also possesses isotopic compositions with OJP-like signature in Pb-Pb and Pb-Nd plots. Together with the northward-decreasing volume of LIP volcanism, the most OJP-like Shatsky Rise isotopic composition coincides thus far with the smaller and youngest end of the rise (North Flank). The trend to more OJP-like signature can be construed as the transition to lower mantle-like composition during the plume head to tail stage of hotspot development, favoring the North Flank-Papanin Ridge connection. However, this interpretation needs to be verified by more and proper samples from the Papanin Ridge.

Alternatively, the trend for the Victoria and Earthwatch seamount compositions to OJP-like isotopic signature may also indicate contamination of their sources by OJP-plume mantle upwelling at that time (~120 Ma), just as inferred for the origin of the central Pacific Basin basalts of similar early Cretaceous age (Janney and Castillo, 1996) and the Cretaceous Pacific lithosphere beneath the Hawaiian North Arch Volcanic Field (Frey et al., 2000). However, given the uncertainty in ages and the small number of samples available from these seamounts, the distinction of whether a more enriched composition is intrinsic to the Shatsky source or reflects a basin wide contamination by OJP magmatism cannot be fully evaluated at this point. Better age control and more geochemical data are required from fresher samples from these two seamounts.

5.3 Alternative origin for the seamounts

The presence of clusters and linear trails of seamounts around and originating from Shatsky Rise could also reflect the interaction of plate boundaries with a long-lived mantle anomaly similar to the South Pacific superswell that may have produced Shatsky-Hess and later, Ontong Java, Manihiki, and Hikurangi plateaus (Sager, 2005). In some cases, volcanic elongate ridges or continuous lines of coeval volcanism extending from a region of intraplate volcanism to a spreading center could develop (O'Connor et al., 1998; 2001), which could be the same situation for the Ojin Rise trail of seamounts that emanate from Shatsky Rise. Most of the seamounts forming Ojin Rise are assembled parallel to magnetic lineations suggesting they formed along a ridge (Nakanishi et al., 1999; Sager et al., 1999). They also have small gravity anomalies, which suggest that they formed near a ridge axis (Sager et al., 1999). In addition, the subcircular morphologies of the Ojin Rise seamounts (Sager et al., 1999; Nakanishi et al., 1999) are reminiscent of some East Pacific and Mid-Atlantic near-ridge seamounts (e.g., Batiza et al., 1989). The enriched MORB (E-MORB)-like trace element abundances, combined with isotopic signatures that trend toward enriched sources are also consistent with a near-ridge seamount origin for the Ojin Rise seamounts in the vicinity of a hotspot (e.g., Hoernle et al., 2011; O'Connor et al., 2012).

On the other hand, shallow, deformation-related volcanism could also occur during plate reorganization (e.g., Line Islands, Sager and Keating, 1984; Musicians Seamounts, O'Connor et al., 2015) or local extension and may have been responsible for the formation of younger seamounts between the massive Shatsky Rise massifs, such as the Cooperation Seamount. However, unlike the purely deformation-related volcanism forming the Musicians Seamounts, the OIB-like major and trace element compositions of the Cooperation Seamount (Tatsumi et al., 1998) combined with the more radiogenic Pb isotopic compositions than MORB require a hotspot-influenced or mixed mantle source input. Cooperation Seamount lies in a northeast-trending basin bounded by the faulted flanks of the TAMU and ORI massifs (Sager et al., 1999). The strong linear morphology of the seamount, which parallels the basin axis and other nearby linear volcanic ridges, also suggests structural control on its formation. This strong linear nature could be associated with rifting between the two massifs soon after they were emplaced (Nakanishi et al., 1999;

Sager et al., 1999). Similar to Ojin Rise and Cooperation Seamount, the high $^{206}Pb/^{204}Pb$-type dredged Manihiki Plateau alkalic rocks were also recovered near the Danger Island Trough and may have possibly formed in a rifting environment (Ingle et al., 2007; Timm et al., 2011; Nakanishi et al., 2015). An extensional environment may have promoted small degrees of melting that tapped the less refractory component in the underlying mantle, followed by possible mixing with depleted shallow mantle.

5.4 Insights into the formation and mantle source evolution of Shatsky-Hess Rise

The formation of Shatsky Rise is unique in many aspects compared to the Ontong Java, Manihiki, Hikurangi, and Kerguelen plateaus. Geophysical studies have shown that Shatsky Rise was built up of discrete volcanoes that progressively become smaller with time and that each massif may have been constructed within a few million years (Sager et al., 1999; 2011; 2013; Nakanishi et al., 1999; Sager, 2005; Zhang et al., 2015). Nevertheless, younger features like basement-top ridges and seamounts also appear to occur on the volcanic massifs (Sager et al., 1999). Based on our new $^{39}Ar/^{40}Ar$ age results from dredged rocks from Toronto Ridge on TAMU and from the eastern summit of ORI, there is evidence that the volcanic edifices may have been built in multiple stages and over an extended period of time, i.e., up to 15 million years (145-129 Ma for TAMU and 134-117 Ma for ORI; Mahoney et al., 2005; Geldmacher et al., 2014; Heaton and Koppers, 2014) after initial formation of the massifs. Interestingly, although based only on few data, the isotopic composition appears to have remained similar throughout the development of each massif [e.g., TN037-D14 vs. Site U1437 (TAMU) and TN037-D9 vs. Site U1350 (ORI); Figs 7-8]. Note that a comparable range in age (118-96 Ma) was also determined on isotopically similar

Hikurangi Plateau dredged basalts (Hoernle et al., 2010). This trend contrasts with that of Hawaiian volcanoes.

As Hawaiian volcanoes migrate over a melting anomaly, they evolve from building a voluminous shield stage of tholeiitic basalt followed by the post-shield stage formed of dominantly alkalic lavas (Clague and Dalrymple, 1987), which is thought to be the end of the shield building stage (Moore and Clague, 1992). After a temporal hiatus, alkalic rejuvenated-stage lavas may erupt. A diagnostic geochemical feature of this evolution is that the alkalic lavas are enriched in highly incompatible elements but they have lower $^{143}Nd/^{144}Nd$ and higher $^{87}Sr/^{86}Sr$ than the tholeiitic shield basalts (Chen and Frey, 1985; Gaffney et al., 2005; Fekiacova et al., 2007). The change to late-shield may also occur shortly before the end of the shield building stage (Moore and Clague, 1992). Whether or not the younger volcanism on TAMU massif represents the end of the shield-building stage or an expression of rejuvenated volcanism similar to Hawaiian volcanoes (e.g., Moore and Clague, 1992; Frey et al., 2000) has an implication on the mode and timing of plateau emplacement and is an interesting question for future investigation. For instance, although the bulk of the TAMU massif was emplaced at 145 Ma, the presence of younger (133.9±2.3 Ma; Geldmacher et al., 2014) flows toward the top of the drilled section at Site U1347 combined with the almost overlapping age (129.42±0.32 Ma) of the isotopically similar Toronto Ridge lavas on top of the massif suggest continued magmatic activity from the same source at 145-130 Ma. Nevertheless, the volcanic sandstone layers separating the younger flows at Site U1347 could represent short temporal hiatuses (Sager et al., 2011).

The similar initial source composition and geochemical evolution supports a plausible connection between Shatsky Rise and Hess Rise, with the latter probably representing either a resurgent plume head pulse (Bercovici and Mahoney, 1994) and/or a triple junction-aided second LIP eruption (Sager, 2005; Davies et al., 2015; O'Connor and Jokat, 2015). Each of these rises could have evolved from plateau-building stage composed of isotopically-depleted tholeiites forming the large massifs to post-plateau building stage consisting of isotopically-enriched trachytes forming the much smaller seamounts, e.g., Shatsky Rise to Cooperation-Earthwatch-Ojin seamount and Hess Rise to Site 465A seamount (Fig. 10). Like Shatsky Rise, a short chain of seamounts of alkaline composition (Wentworth Seamount Chain, Fig. 1b) extending SE from southern Hess Rise, i.e. from Site 465, (intersecting with the much younger Hawaiian-Emperor chain), seems to show an age progression that is consistent with being a classical hotspot track associated with the Hess Rise (Pringle and Dalrymple, 1993). Although the results of this study cannot unequivocally provide a direct link between the plateaus and seamount volcanism, further investigation of these similar trends of mantle source variation, not only between Shatsky and Hess Rise but also Ontong Java, Manihiki, and Hikurangi plateaus could lead to a better understanding of the origin, evolution, and emplacement mode of most Pacific oceanic plateaus.

6. Conclusions

The isotopic similarity between the low- $^{206}Pb/^{204}Pb$ Site 464 tholeiites from Hess Rise and the tholeiitic Shatsky Rise plateau basalts are consistent with a common source. The seamounts, except for the Toronto Ridge, cannot be directly linked to Shatsky Rise. The presently available data do not allow us to rule out either Cooperation-Ojin Rise or North Flank-Papanin Ridge connection between the two plateaus. More sampling and data, particularly from North Flank and Papanin Ridge, are needed to better constrain their relationship with Shatsky Rise.

The seamount volcanism could be an expression of source heterogeneity or geochemical evolution of the Shatsky-Hess mantle source with time. The isotopic compositional variation from depleted MORB-like composition to FOZO- or OJP-like to HIMU-like could reflect the transition from the plume head (dominated by entrained shallow mantle) to the plume tail (dominated by lower mantle material comprising the plume axis). Alternatively, the isotopically enriched mantle components may have been tapped during intermittent volcanism over a long-lived mantle anomaly similar to the present-day South Pacific Superswell, interacting with triple junction and tectonic deformation. Further age and geochemical data are needed to fully evaluate these possibilities.

New $^{39}Ar/^{40}Ar$ age dating confirms that the TAMU Massif of Shatsky Rise may have been built in several stages and over a period of about 15 m.y. The isotopic data from the younger Toronto Ridge reveal that the source composition, however, appears to have remained constant over the entire history of formation of the TAMU Massif.

Acknowledgements

We acknowledge the assistance of many people who helped us in collecting the samples: the captain, technical staff, and crew of R/V *Thomas G. Thompson,* fellow rock describers Atsushi Horio and Glenn Brown, the Earthwatch (Jim Barkes, Diane Boyers, Jody Fairchild, Mary Lewis, Maureen McColl and Rowena Pike) and student (Tucker Burkhart, Robert Cherevatry, Jim Finlayson and Andrew Mikitchook) volunteers during the TN037 cruise. M. T. is indebted to: late Prof. John Mahoney of University of Hawaii for advice and earlier discussions of analytical results; R. Senda and Q. Chang for assistance in the analytical work at JAMSTEC; and M. Nakanishi and A. Klaus for helpful discussions on the interpretations of geophysical data. Analytical work at GEOMAR and University of Kiel was supported by Silke Hauff and Ulrike Westernströer. This manuscript benefited very much from the editorial handling of M. Norman and the critical reviews and comments of F. Frey, S. Huang, C. Neal, A. Saunders and an anonymous reviewer. The TN037 cruise costs were supported by National Science Foundation grant OCE93-14229 to W. Sager and supplemented by Earthwatch. K.H. and K.Hy. acknowledge funding by the German Research Council (DFG grant HO1833/211). Hess Rise DSDP samples were provided by the International Ocean Discovery Program (IODP).

Figure captions

Figure 1. a) Bathymetric chart of Shatsky Rise with previous ocean drilling sites and R/V Thompson expedition TN037 dredge hauls modified after Sager, et al., 2011. Ages from ^{40}Ar-^{39}Ar dating (Mahoney et al., 2005; Koppers, 2010; Geldmacher et al., 2014; Heaton and Koppers, 2014; this study) and range in seafloor magnetic anomalies (Sager et al., 1999; Nakanishi et al., 1999) are shown. b) Regional overview map with selected magnetic lineations (dashed lines), location of DSDP drill sites on Hess Rise, and reconstructed paths of volcanism (hotspot tracks) with assumed ages based on magnetic data (after Sager, 2005) combined with age data for the Wentworth

Seamount Chain (WC) (Pringle and Dalrymple, 1993). The dashed arrow represents a possible second hotspot track between Shatsky and Hess Rise, following the Ojin Rise Seamount trail (e.g., Sager et al., 1999; Nakanishi et al., 1999).

Figure 2. Bivariate plots of selected major element oxides vs. MgO for the TN037 dredged volcanic rocks (gray symbols; Tatsumi et al., 1998), Shatsky Rise (Sano et al., 2012), and Hess Rise (Seifert et al., 1981). Samples selected for this study are highlighted by the same but colored and bigger symbols.

Figure 3. Bivariate plots of Nb, Zr, Nb/Y, Zr/Y and chondrite-normalized Sm/Yb , Ce/Yb and Nb/Yb for the least altered Ojin (D1), Earthwatch (D4), and Cooperation (D11) seamount samples compared with drilled Hess Rise and Shatsky Rise basalts data from the TAMU, ORI, and Shirshov massifs (Seifert et al., 1981; Sano et al., 2012). The Zr-Nb plot and data fields for mid-ocean ridge basalts (MORB), ocean island basalts (OIB), Ontong Java Plateau (OJP) and Iceland are from Fitton and Godard (2004). The plume vs. MORB mantle discrimination plot, Zr/Y-Nb/Y, showing the Iceland Array is from Fitton et al. (1997).

Figure 4. High-resolution incremental heating $^{40}Ar/^{39}Ar$ age analyses for the TN037 dredged rocks (left column) and cumulative amount of ^{39}Ar released plotted against K/Ca ratios (right column) for Toronto Ridge (top), Cooperation Seamount (middle), and ORI Massif (bottom). The reported $^{40}Ar/^{39}Ar$ ages are weighted age estimates and errors on the 95% confidence level including 0.1-0.2% (1σ) deviations in the J-value. All samples were monitored against FCT-NM sanidine (28.201 ± 0.081 Ma, 1σ; Kuiper et al., 2008). Data are listed in Table 4.

Figure 5. Chondrite-normalized rare earth element patterns for Hess Rise, Ojin Rise (D1), Earthwatch (D4), and Cooperation (D11) seamount samples compared to those of phosphorites (Garnit et al., 2012), and Pacific Fe-oxide rich sediments (Kato et al., 2011) shown at the bottom panel. Samples without the "D" prefix in their labels are from Hess Rise drill sites. Chondrite values are from McDonough and Sun (1995).

Figure 6. Primitive mantle-normalized incompatible trace element patterns for Cooperation Seamount (D11) and least altered Ojin Rise (D1) and Earthwatch (D4) seamounts (top panel) samples compared to those of Manihiki (Ingle et al., 2007) and OJP (Tejada et al., 1996) alkalic rocks, most trace element-enriched Shirshov (Sano et al., 2012), and average Kwaimbaita and Singgalo-type edifice-forming tholeiites inferred to be products of plume head mantle melting (Tejada et al., 2002). Both the Singgalo and Shirshov basalts represent the latest plateau-forming eruption products of OJP and Shatsky Rise, respectively, presumed to show transitional composition closest to those of the seamount samples. Primitive mantle values are from McDonough and Sun (1995).

Figure 7. Plots of initial $\varepsilon_{Nd}(t)$ vs. $\varepsilon_{Hf}(t)$ and $(^{206}Pb/^{204}Pb)_t$ for Hess Rise (circles), Toronto Ridge (open square), and Ojin (diamonds), Earthwatch (filled squares), and Cooperation (triangles) seamount samples, together with fields for modern MORBs (White et al., 1987; Mahoney et al., 1994; Schiano et al., 1997; Chauvel and Blichert-Toft, 2001; Andres et al., 2002; Escrig et al., 2004; Janney et al., 2005; Agranier et al., 2005; Debaille et al., 2006; Hamelin et al., 2011 and *PetDB* database), Shatsky Rise (Mahoney et al., 2005; Heydolph et al., 2014), OJP (Tejada et al., 2002; 2004; 2013), Manihiki Plateau (Mahoney and Spencer, 1991; Ingle et al., 2007; Hoernle et al.,

2010; Timm et al., 2011), Hikurangi Plateau (Hoernle et al., 2010), Nauru Basin (Castillo et al., 1991); ODP Site 801 Jurassic alkalic basalts (Castillo et al., 1992; Hauff et al., 2003). Also shown are age-corrected and estimated 120 Ma mantle source fields (except for Hf isotopes) for Mangaia Group islands (Vidal et al., 1984; Palacz and Saunders, 1986; Nakamura and Tatsumoto, 1988; Chauvel et al., 1992; Hanyu et al., 2011), Pitcairn (Eisele et al., 2002), Samoa (Patchett and Tatsumoto, 1980; Hart et al., 2004), Rarotonga (Hanyu et al., 2011), and Louisville (Cheng et al., 1987; Beier et al., 2011; Vanderkluysen et al., 2014; Williams et al., 2014) seamounts. The 120 Ma mantle source fields are drawn using the following $^{147}Sm/^{144}Nd$ and $^{238}U/^{204}Pb$ values: 0.24 and 5 for MORB source (White, 1993; Mahoney et al., 1998) and 0.20 and 22 for the Mangaia Group source (Chauvel et al., 1992). Abbreviations: MP= Manihiki Plateau; HP= Hikurangi Plateau; KK= Kroenke-Kwaimbaita; Sg= Singgalo

Figure 8. Initial $(^{208}Pb/^{204}Pb)_t$ vs. $(^{206}Pb/^{204}Pb)_t$ (a) and $(^{207}Pb/^{204}Pb)_t$ vs. $(^{206}Pb/^{204}Pb)_t$ (b) for Hess Rise, Toronto Ridge, and Earthwatch, Ojin Rise, and Cooperation Seamount samples. Symbols, fields and data sources are as in Fig. 7. The Th/U values used for age-adjustments of Pb isotopic compositions are 2.5 for MORB (White 1993) and 3.2 for the Mangaia Group (Chauvel et al. 1992).

Figure 9. Compilation of ages derived from ^{40}Ar-^{39}Ar and biostratigraphy for Shatsky (Mahoney et al., 2005; Koppers, 2010; Geldmacher et al., 2014; Heaton and Koppers, 2014; this study) and Hess Rise (Thiede et al., 1981; Pringle and Dalrymple, 1993) compared to Ontong Java Plateau (Mahoney et al., 1993; Tejada et al., 1996; 2002; Sikora and Bergen, 2004), Manihiki Plateau (Ingle et al., 2007; Hoernle et al., 2010; Timm et al., 2011) and Hikurangi Plateau (Hoernle et al., 2010).

Figure 10. Initial $(^{206}Pb/^{204}Pb)_t$, $(^{167}Hf/^{177}Hf)_t$, and $(^{143}Nd/^{144}Nd)_t$ vs. age plots for Shatsky Rise (Heydolph et al., 2014), Hess Rise, and the seamounts. Also shown are model evolution curves for OJP, primitive mantle (PM), and MORB sources (from Tejada et al., 2004), and the evolution band for Shatsky Rise mantle source with the solid curve representing the average for TAMU Massif data and the width of the band representing the lowest and highest values derived from all Shatsky Rise data (Heydolph et al., 2014). Parent-daughter ratios used for Shatsky data ($^{147}Sm/^{144}Nd$= 0.2873; $^{176}Lu/^{177}Hf$= 0.0996; $^{238}U/^{204}Pb$= 14.1 and $^{232}Th/^{204}Pb$= 34.9) were derived by estimating the source composition using simple modal batch melting equation assuming 15% melting (Sano et al., 2012) and mineral proportions of 0.6ol: 0.2opx: 0.15cpx: 0.05gt and 0.15ol :0.3opx: 0.25cpx: 0.3gt for mantle source and melting modes, respectively. Partition coefficients used are from Kennedy et al. (1993), Green (1994) and Hauri et al. (1994) for Lu. Symbols are the same as in Figs. 7-8; smaller symbols represent the estimated back-tracked (age-corrected) composition to 145 Ma, with the bars representing the range of composition for each seamount. Arrows represent the similar source variation trends between Shatsky Rise and Hess Rise.

REFERENCES

Agranier, A., Blichert-Toft, J., Graham, W.D., Debaille, V., Schiano, P. and Albarede, F. (2005) The spectra of isotopic heterogeneities along the mid-Atlantic Ridge. *Earth Planet. Sci. Lett.* **238**, 96-109.

Andres, M., Blichert-Toft, J. and Schilling, J.G. (2002) Hafnium isotopes in basalts from the southern Mid-Atlantic Ridge from 40^{o}S to 55^{o}S: Discovery and Shona plume-ridge interactions and the role of recycled sediments. *Geochem. Geophys. Geosyst.* **3**, 8502, doi:10.1029/2002GC000324.

Batiza, R., Fox, P. J., Vogt, P. R., Cande, S. C., Grindlay, N. R., Melson, W. G. and O'Hearn, T. (1989) Morphology, abundance, and chemistry of near-ridge seamounts in the vicinity of the Mid-Atlantic ridge ~26^{o}S. *J. Geology* **97**, 209-220.

Beier, C., Vanderkluysen, L., Regelous, M., Mahoney,J. J. and Garbe-Schönberg, D. (2011) Lithospheric control on geochemical composition along the Louisville Seamount Chain. *Geochem. Geophys. Geosyst.,* **12**, Q0AM01, doi:10.1029/2011GC003690.

Beiersdorf, H., Bach, W., Duncan, R., Erzinger, J. and Weiss, W. (1995) New evidence for the production of EM-type ocean island basalts and large volumes of volcaniclastites during the early history of the Manihiki Plateau. *Mar. Geol*. **122**, 181-205.

Bercovici, D. and Mahoney, J. (1994) Double flood-basalt events and the separation of mantle-plume heads at the 660 km discontinuity. *Science* **266**, 1367-1369.

Bouvier, A., Jeffrey, D., Vervoort, P. and Patchett, J. (2008) The Lu-Hf and Sm-Nd isotopic composition of CHUR: Constraints from unequilibrated chondrites and implications for the bulk composition of terrestrial planets. *Earth Planet. Sci. Lett.* **273**, 48-57.

Castillo, P. R., Carlson, R. W. and Batiza, R. (1991) Origin of Nauru Basin igneous complex: Sr, Nd, and Pb isotopes and REE constraints. *Earth Planet. Sci. Lett.* **103,** 200-213.

Castillo, P. R., Floyd, P. A. and France-Lanord, C. (1992) Isotope and geochemistry of Leg 129 basalts: implications for the origin of the widespread Cretaceous volcanic event in the Pacific. In *Proceedings ODP Scientific Results 129* (eds. R. L. Larson, Y. Lancelot, et al.). Ocean Drilling Program, College Station, TX. pp. 405-413.

Chandler, M. T., Wessel, P. and Taylor, B. (2015) Tectonic reconstructions in magnetic quiet zones: Insights from the Greater Ontong Java Plateau. In *The Origin, Evolution, and Environmental Impact of Oceanic Large Igneous Provinces* (eds. C. R. Neal, W. W. Sager, T. Sano and E. Erba). Special Paper 511 (8), Geological Society of America Special Paper 511, p. 185-193.

Chang, Q., Shibata, T., Shinotsuka, K., Yoshikawa, M., and Tatsumi, Y. (2002) Precise determination of trace elements in geological standard rocks using inductively coupled plasma mass spectrometry (ICP-MS). *Front. Res. Earth Evoln.* **1,** 357-362.

Chauvel, C. and Blichert-Toft, J. (2001) A hafnium isotope and trace element perspective on melting of the depleted mantle. *Earth Planet. Sci. Lett.* **190**, 137-151.

Chauvel, C., Hoffman, A. W. and Vidal, P. (1992) HIMU-EM: The French Polynesian connection. *Earth Planet. Sci. Lett.* **110**, 99-119.

Chen, C. and Frey, F. (1985) Trace element and isotopic geochemistry of lavas from Haleakala volcano, East Maui, Hawaii: Implications for the origin of Hawaiian basalts. *J. Geophys. Res.* **90,** 8743-8768.

Cheng, Q., Park, K.-H., MacDougall, J. D., Zindler, J. D., Lugmair, A., Hawkins, G. W., Lonsdale, P. and Staudigel, H. (1987) Isotopic evidence for a hotspot origin of the Louisville seamount chain. In *Seamounts, Islands, and Atolls* (eds. B. Keating, P. Fryer, R. Batiza and G. Boehlert). *Geophysical Monograph, American Geophysical Union* **43**, 283-296.

Clague, D. A. and Dalrymple, G. B. (1987) The Hawaiian-Emperor volcanic chain, Part 1. *USGS Prof. Paper* **1350-1**, 5-54.

Coffin, M. F. and Eldholm, O. (1994) Large igneous provinces: Crustal structure, dimensions, and external consequences. *Rev. Geophys.* **32**, 1-36.

Coffin, M. F., Pringle, M. S., Duncan, R. A., Gladczenko, T. P., Storey, M., Muller, R. D. and Gahagan, L. A. (2002) Kerguelen hotspot magma output since 130 Ma. *J. Petrol*. **43**, 1121-1139.

Cullen, D. J. and Burnett, W. C. (1986) Phosphorite associations on seamounts in the tropical southwest Pacific Ocean. *Mar. Geol.* **71**, 215-236.

Davies, D. R., Goes, S. and Sambridge, M. (2015) On the relationship between volcanic hotspot locations, the reconstructed eruption sites of large igneous provinces and deep mantle seismic structure. *Earth Planet. Sci. Lett.* **411**, 121-130.

Davy, B., Hoernle, K. and Werner, R. (2008) Hikurangi Plateau: Crustal structure, rifted formation, and Gondwana subduction history. *Geochem. Geophys. Geosys.* **9**, n/a–n/a, doi: 10.1029/2007GC001855

Debaille, V., Blichert-Toft, J., Agranier, A., Doucelance, R., Schiano, P. and Albarede, F. (2006) Geochemical component relationships in MORB from the Mid-Atlantic Ridge, 22-358N. *Earth Planet. Sci. Lett.* **241**, 844-862.

Eisele, J., Sharma, M., Galer, S.J.G., Blichert-Toft, J., Devey, C.W. and Hoffman, A.W. (2002) The role of sediment recycling in EM-1 inferred from Os, Pb, Hf, Nd, Sr isotope and trace element systematics of the Pitcairn hotspot. *Earth Planet. Sci. Lett.* **196**, 197-212.

Escrig, S., Capmas, F., Dupre, B. and Allegre, J.C. (2004) Osmium isotopic constraints on the nature of the DUPAL anomaly from Indian mid-ocean ridge basalts. *Nature* **431**, 59-63.

Fekiacova, Z., Abouchami, W., Galer, S. J. G., Garcia, M. O. and Hoffman, A. W. (2007) Origin and temporal evolution of Ko'olau Volcano, Hawai'i: Inferences from isotope data on the Ko'olau Scientific Drilling Project (KSDP), the Honolulu Volcanics and ODP Site 843. *Earth Planet. Sci. Lett.* **261**, 65-83.

Fitton, J. G. and Godard, M. (2004) Origin and evolution of magmas on the Ontong Java Plateau. In *Origin and Evolution of the Ontong Java Plateau* (eds. J. G. Fitton, J. J. Mahoney, P. J. Wallace and A. D. Saunders) Geological Society of London Special Publication 229, p. 151-178.

Fitton, J. G., Saunders, A. D., Norry, M. J., Hardarson, B. S. and Taylor, R. N. (1997) Thermal and chemical structure of the Iceland plume. *Earth Planet. Sci. Lett.* **153**, 197-208.

Frey, F. A., Clague, C., Mahoney, J. J. and Sinton, J. M. (2000) Volcanism at the edge of the Hawaiian Plume: Petrogenesis of submarine alkalic lavas from the North Arch Volcanic Field. *J. Petrol.* **41**, 667-691.

Gaffney, A. M., Nelson, B. K. and Blichert-Toft, J. (2005) Melting in the Hawaiian plume at 1-2 Ma as recorded at Maui Nui: The role of eclogite, peridotite, and source mixing. *Geochem. Geophys. Geosyst.* **6**, Q10L11, doi:10.1029/2005GC000927.

Garbe-Schönberg, C. D. (1993) Simultaneous determination of thirty-seven trace elements in twenty-eight international rock standards by ICP-MS. *Geostandards Newsletter* **17**, 81-97.

Garnit, H., Bouhlel, S., Barca, D. and Chtara, C. (2012) Application of LA-ICPMS to sedimentary phosphatic particles from Tunisian phosphorite deposits: Insights from trace elements and REE into paleo-depositional environments. *Chem. der Erde* **72**, 127-139.

Geldmacher, J., Van den Bogaard, P., Heydolph, K. and Hoernle, K. (2014) The age of Earth's largest volcano: Tamu Massif on Shatsky Rise (northwest Pacific Ocean). *Int. J. Earth. Sci. (Geol. Rundsch.)* **103,** 2351-2357, DOI 10.1007/s00531-014-1078-6.

Green, T. H. (1994) Experimental studies of trace element partitioning applicable to igneous petrogenesis – Sedona 16 years later. *Chem. Geol.* **117**, 1-36.

Hamelin, C., Dosso, L., Hanan, B., Moreira, M., Kositsky, A.P. and Thomas, M.Y. (2011) Geochemical portray of the Pacific Ridge: New isotopic data and statistical techniques. *Earth Planet. Sci. Lett.* **302**, 154-162.

Hanyu, T., Tatsumi, Y., Senda, R., Miyazaki, T., Chang, Q., Hirahara, Y., Takahashi, T., Kawabata, H., Suzuki, K., Kimura, J-I. and Nakai, S. (2011) Geochemical characteristics and origin of the HIMU reservoir: A possible mantle plume source in the lower mantle. *Geochem. Geophys. Geosys.* **12**, Q0AC09, doi:10.1029/2010GC003252.

Hanyu, T., Shimizu, K. and Sano, T. (2015b) Noble gas evidence for the presence of recycled material in magma sources of Shatsky Rise. In *The Origin, Evolution, and Environmental Impact of Oceanic Large Igneous Provinces* (eds. C. R. Neal, W. W. Sager, T. Sano and E. Erba). Special Paper 511 (3), Geological Society of America Special Paper 511, p. 57-67.

Hanyu, T., Tejada, M. L. G., Shimizu, K., Ishikawa, A., Kimura, J.-I., Chang, Q., Senda, R., Miyazaki, T., Goto, K. and Ishizuka, O. (2015a) Remelting of Ontong Java Plateau lithosphere. In *2015 Annual Goldschmidt Conference Abstracts,* 1175.

Hart, S. R., Hauri, E. H., Oschmann, L. A. and Whitehead, J. A. (1992) Mantle plumes and entrainment: Isotopic evidence. *Science* **256**, 517-520.

Hart, S.R., Coetze, M., Workman, R.K., Blusztajn, J., Johnson, K.T. M., Sinton, J.M., Steinberger, B. and Hawkins, J.W. (2004) Genesis of the Western Samoa seamount province: age, geochemical fingerprint and tectonics. *Earth Planet. Sci. Lett.* **227**, 37-56.

Hauff, F., Hoernle, K. and Schmidt, A. (2003) Sr-Nd-Pb composition of Mesozoic Pacific oceanic crust (Site 1149 and 801, ODP Leg 185): Implications for alteration of ocean crust and input into the Izu-Bonin-Mariana subduction system. *Geochem. Geophys. Geosys.* **8**, doi:10.1029/2002GC000421.

Hauri, E.H., Wagner, T.P. and Grove, T.L. (1994) Experimental and natural partitioning of Th, U, Pb and other trace elements between garnet, clinopyroxene and basaltic melts. *Chem. Geol.* **117**, 149-166*. doi: 10.1016/0009-2541(94)90126-0*

Heaton, D. E. and Koppers, A. A. P. (2014) Constraining the rapid construction of TAMU Massif at an ~145 Myr old triple junction, Shatsky Rise. Annual V. M. Goldschmidt Conference (abstr.) # 948.

Hein, J. R., Yeh, H-W., Gunn, S. H., Sliter, W. V., Benninger, L. M. and Wang, C-H. (1993) Two major Cenozoic episodes of phosphogenesis recorded in equatorial Pacific seamount deposits. *Paleoceanography* **8**, 293-311.

Heydolph, K., Murphy, D. T., Geldmacher, J., Romanova, I. V., Greene, A., Hoernle, K., Weis, D. and Mahoney, J. (2014) Plume versus plate origin for the Shatsky Rise oceanic plateau (NW Pacific): Insights from Nd, Pb, and Hf isotopes. *Lithos* **200-201**, 49-63.

Hoernle, K., Hauff, F., Bogaard, P., Werner, R., and Mortimer, N. (2005) The Hikurangi oceanic plateau: Another large piece of the largest volcanic event on earth. *Goldschmidt Conference*

Abstracts, Moscow, Idaho, USA, May 21-25, Geochimica et Cosmochimica Acta, Vol.69 (10), Supplement 1, A96.

Hoernle, K., Hauff, F., Werner, R., van den Bogaard, P., Timm, C., Coffin, M., Mortimer, N., and Davy, B. (2008) A Similar Multi-stage Geochemical Evolution for the Manihiki, Hikurangi and Ontong Java Plateaus? *AGU Fall Meeting, San Fransisco, USA, December 14-19, Eos Trans. AGU, 89(53), Fall Meet. Suppl., Abstract V23H-05*.

Hoernle, K., Timm, C., Hauff, F., Rüpke, L., Werner, R., Bogaard, P. v. d., Michael, P. J., Coffin, M., Mortimer, N. N., and Davy, B. W. (2009) New Results for the Multi-stage Geochemical Evolution of the Manihiki and Hikurangi Plateaus. *AGU Fall Meeting, San Fransisco, USA, December 14-18, Eos Trans. AGU, 90 (53), Fall Meet. Suppl., Abstract V51H-03, Invited Talk*.

Hoernle, K., Hauff, F., van den Bogaard, P., Werner, R., Mortimer, N., Geldmacher, J., Garbe-Schonberg, D. and Davy, B. (2010) Age and geochemistry of volcanic rocks from the Hikurangi and Manihiki oceanic Plateaus. *Geochim. Cosmochim. Acta*, **74,** 7196-7219.

Hoernle, K., Hauff, F., Kokfelt, T. F., Haase, K., Garbe-Schönberg, D., and Werner, R. (2011) On- and off-axis chemical heterogeneities along the South Atlantic Mid-Ocean-Ridge (5-11°S): Shallow or deep recycling of ocean crust and/or intraplate volcanism? *Earth and Planetary Science Letters* **306**, 86-97.

Huang, S., Regelous, M., Thordarson, T. and Frey, F. A. (2005) Petrogenesis of lavas from Detroit Seamount: Geochemical differences between Emperor Chain and Hawaiian volcanoes. *Geochem. Geophys. Geosyst.* **6,** 52 p, Q01L06, doi:10.1029/2004GC000756.

Husen, A., Almeev, R. R., Holtz, F., Koepke, J., Sano, T. and Mengel, K. (2013) Geothermobarometry of basaltic glasses from the Tamu Massif, Shatsky Rise oceanic plateau. *Geochem. Geophys. Geosyst.* **14,** 3908-3928, doi:10.1002/ggge.20231.

Ingle, S., Mahoney, J. J., Sato, H., Coffin, M. F., Kimura, J-I., Hirano, N. and Nakanishi, M. (2007) Depleted mantle wedge and sediment fingerprint in unusual basalts from the Manihiki Plateau, central Pacific Ocean. *Geology* **35,** 595-598.

Jackson, M. G. and Carlson, R. W. (2011) An ancient recipe for flood-basalt genesis. *Nature* **476**, 316-319.

Janney, P. E. and Castillo, P. R. (1996) Basalts from the Central Pacific Basin: Evidence for the origin of Cretaceous igneous complexes in the Jurassic western Pacific. *J. Geophys. Res.* **101**, 2875-2893.

Janney, P.E., Le Roex, A.P. and Carlson, R.W. (2005) Hafnium isotopes and trace element constraints on the nature of mantle heterogeneity beneath the central Southwest Indian Ridge (13^{o}E to 47^{o}E). *J. Petrol.* **46**, 2427-2464.

Jarvis, I., Burnett, W. C., Nathan, Y., Almbaydin, F. S. M., Attia, A. K. M., Castro, L. N., Flicoteaux, R., Hilmy, M. E., Husain, V., Qutawnah, A. A., Serjani, A. and Zanin, Y. N. (1994) Phosphorite geochemistry: State-of-the-art and environmental concerns. *Ecl. Geol. Helv.* **87**, 643-700.

Kato, Y., Fujinaga, K., Nakamura, K., Takaya, Y., Kitamura K., Ohta, J., Toda, R., Nakashima R., and Iwamori H. (2011) Deep-sea mud in the Pacific Ocean as a potential resource for rare-earth elements. *Nat. Geosci*. **4**, 535-539.

Kennedy, A. K., Lofgren, G. E. and Wasserburg, G. J. (1993) An experimental study of trace element partitioning between olivine, orthophyroxene, and melt in chondrules: equilibrium values and kinetic effects. *Earth Planet. Sci. Lett.* **115**, 177-195.

Kimura, J-I. and Kawabata, H. (2015) Ocean Basalt Simulator version 1 (OBS1): Trace element mass balance in adiabatic melting of a pyroxenite-bearing peridotite. *Geochem. Geophys. Geosyst.* **16,** 267–300, doi:10.1002/2014GC005606.

Konter, J. G., Hanan, B. B., Blichert-Toft, J., Koppers, A. P., Plank, T. and Staudigel, H. (2008) One hundred million years of mantle geochemical history suggest the retiring of mantle plumes is premature. *Earth Planet. Sci. Lett.* **275,** 285-295.

Koppers, A. A. P. (2010) Massive basalt flows on the southern flank of Tamu Massif, Shatsky Rise: A reappraisal of ODP Site 1213 basement units. In *Proceedings of the Integrated Ocean Drilling Program 324* (eds. Sager, W., Sano, T., Geldmacher, J. et al., IODP, Tokyo, doi:10.2204/ iodp.proc.324.2010.

Koppers, A. A. P., Staudigel, H. and Wijbrans, J. R. (2000) Dating crystalline groundmass separates of altered Cretaceous seamount basalts by the $^{40}Ar/^{39}Ar$ incremental heating technique. *Chem. Geol.* **166**, 139-158.

Koppers, A. A. P., Duncan, R. A. and Steinberger, B. (2004) Implications of a nonlinear $^{40}Ar/^{39}Ar$ age progression along the Louisville seamount trail for models of fixed and moving hot spots. *Geochem. Geophys. Geosys.* **5**, n/a–n/a, doi: 10.1029/2003GC000671

Koppers, A. A. P., Gowen, M. D., Colwell, L. E., Gee, J. S., Lonsdale, P. F., Mahoney, J. J., and Duncan, R. A. (2011) New $^{40}Ar/^{39}Ar$ age progression for the Louisville hot spot trail and implications for inter–hot spot motion. *Geochem. Geophys. Geosys.* **12**, n/a–n/a, doi: 10.1029/2011GC003804.

Kroenke, L. W. (1996) Plate tectonic development of the western and southwestern Pacific: Mesozoic to the present. In *The origin and evolution of Pacific Island biotas, New Guinea to Eastern Polynesia: patterns and processes* (eds. Keast, A. and Miller S. E.). SPB Academic Publishing, Amsterdam, Netherlands. pp. 19-34.

Kroenke, L. W. and W. W. Sager (1993) The formation of oceanic plateaus on the Pacific plate. *Eos, Trans. Am. Geophys. Union* **74**, 43, 443.

Kuiper, K. F., Deino, A., Hilgen, F. J., Krijgsman, W., Renne, P. R. and Wijbrans, J. R. (2008) Synchronizing rock clocks of earth history. *Science* **320**, 500–504, doi: 10.1126/science.1154339.

Larson, R. L., Steiner, M. B. Erba, E. and Lancelot, Y. (1992) Paleolatitudes and tectonic reconstructions of the oldest portion of the Pacific Plates: A comparative study. In *Proceedings Ocean Drilling Program Scientific Results 129* (eds. R. L. Larson, Y. Lancelot, et al.,) Ocean Drilling Program, College Station, TX. pp. 615-631.

Lin, S-C. and van Keken P. E. (2005) Multiple volcanic episodes of flood basalts caused by thermochemical mantle plumes. *Nature* **436**, 250-252.

Mahoney, J. J. (1987) An isotopic survey of Pacific oceanic plateaus: implications for their nature and origin. In *Seamounts, Islands, and Atolls* (eds. B. Keating, P. Fryer, R. Batiza and G. Boehlert) *Am. Geophys. Union Geophys. Monogr.* **43**, pp. 207-220.

Mahoney, J. J. and Spencer, K. J. (1991) Isotopic evidence for the origin of the Manihiki and Ontong Java oceanic plateaus. *Earth Plane. Sci. Lett.* **104**, 196-210.

Mahoney, J. J., Storey, M., Duncan, R. A., Spencer, K. J. and Pringle, M. (1993) Geochemisty and geochronology of the Ontong Java Plateau. In *The Mesozoic Pacific. Geology, Tectonics, and Volcanism* (eds. M. Pringle, W. Sager, et al.). Geophysical Monograph **77**, American Geophysical Union. pp. 233-261.

Mahoney, J. J., Sinton, J. M., Kurz, M. D., MacDougall, J. D., Spencer, K. J. and Lugmair, G. W. (1994) Isotope and trace element characteristics of a super-fast spreading ridge: East Pacific Rise, 13-23^{o}S. *Earth and Planetary Science Letters* **121**, 173-193.

Mahoney, J. J., Frei, R., Tejada, M. L. G., Mo, X. X., Leat, P. T. and Nägler, T. F. (1998) Tracing the Indian Ocean mantle domain through time: Isotopic results from old West Indian, East Tethyan, and South Pacific seafloor. *Journal of Petrology* **39**, 1285-1306.

Mahoney, J. J., Duncan, R. A., Tejada, M. L. G., Sager, W. W. and Bralower, T. J. (2005) Jurassic-Cretaceous boundary age and mid-ocean-ridge-type mantle source for Shatsky Rise. *Geology* **33,** 185–188.

McDonough, W. F. and Sun, S.-s. (1995) The composition of the Earth. *Chem. Geol.* **120**, 223-253.

Min, K., Mundil, R., Renne, P.R. and Ludwig, K.R. (2000) A test for systematic errors in 40Ar/39Ar geochronology through comparison with U/Pb analysis of a 1.1-Ga rhyolite: *Geochimica et Cosmochimica Acta* **64**, 73–98. doi: 10.1016/S0016-7037(99)00204-5.

Moore, J. G. and Clague, D. A. (1992) Volcano growth and evolution of the island of Hawaii. *Geol. Soc. Am. Bull.* **104**, 1471-1484.

Nakamura, Y. and Tatsumoto, M. (1988) Pb, Nd, and Sr isotopic evidence for a multicomponent source for rocks of Cook-Austral Islands and heterogeneities of mantle plumes. *Geochimica et Cosmochimica Acta* **52**, 2909-2924.

Nakanishi, M., Tamaki, K. and Kobayashi, K. (1989) Mesozoic magnetic lineations and seafloor spreading history of the northwestern Pacific. *J. Geophys. Res.* **94**, 15437-15462.

Nakanishi, M., Sager, W. W. and Klaus, A. (1999) Magnetic lineations within Shatsky Rise, northwest Pacific Ocean: Implications for hot spot-triple junction interaction and oceani plateau formation. *J. Geophys. Res.* **104,** 7539-7556.

Nakanishi, M., Nakamura, Y., Coffin, M. F., Hoernle, K., and Werner, R. (2015) Topographic expression of the Danger Islands Troughs and implications for the tectonic evolution of the

ACCEPTED MANUSCRIPT

Manihiki Plateau, western equatorial Pacific Ocean. In *The Origin, Evolution, and Environmental Impact of Oceanic Large Igneous Provinces* (eds. C. R. Neal, W. W. Sager, T. Sano and E. Erba). Special Paper 511 (11), Geological Society of America Special Paper 511, p. 195-220.

Nobre-Silva, I. G., Weis, D., Barling, J. and Scoates, J. (2009) Leaching systematics and matrix elimination for the determination of high-precision Pb isotope compositions of ocean island basalts. *Geochem. Geophys. Geosyst.* **10,** 23 pp, doi:10.1020/2009GC002537.

Nobre-Silva, I. G., Weis, D. and Scoates, J. (2010) Effects of acid leaching on the Sr-Nd-Hf isotopic compositions of ocean island basalts. *Geochem. Geophys. Geosyst.* **11,** 20 pp, doi:10.1029/2010GC003176.

O'Connor, J. M. and Duncan, R. A. (1990) Evolution of the Walvis Ridge-Rio Grande Rise hot spot system: implications for African and South American plate motions over plumes. *J. Geophys. Res*. **95**, 17475-17502.

O'Connor, J. and Jokat, W. (2015) Tracking the Tristan-Gough mantle plume using discrete chains of intraplate volcanic centers buried in the Walvis Ridge. *Geology* **43**, 715-718.

O'Connor, J. M., Stoffers, P. and Wijbrans, J. R. (1998) Migration rate of volcanism along the Foundation Chain, SE Pacific. *Earth Planet. Sci. Lett*. **164**, 41-59.

O'Connor, J. M., Stoffers, P. and Wijbrans, J. R. (2001) En echelon volcanic elongate ridges connecting intraplate Foundation Chain volcanism to the Pacific-Antarctic spreading center. *Earth Planet. Sci. Lett*. **189**, 93-102.

O'Connor, J. M., Jokat, W., le Roex, A. P., Class, C., Wijbrans, J. R., Kesling, S., Kuiper, K.F. and Nebel, O. (2012) Hotspot trails in the South Atlantic controlled by plume and plate tectonic processes. *Nat. Geosci.* **5**, 735-738.

O'Connor, J. M., Hoernle, K., Muller, R. D., Morgan, J. P., Butterworth, N. P., Hauff, F., Sandwell, D. T., Jokat, W., Wijbrans, J. R. and Stoffers, P. (2015) Deformation-related volcanism in the Pacific Ocean linked to the Hawaiian-Emperor bend. *Nat. Geosci*. **8**, 393-397.

Ogg, J.G. (2012) Geomagnetic Polarity Time Scale. In *The Geologic Time Scale* (eds. F. M. Gradstein, J. G. Ogg, M.D. Schmitz and G. M. Ogg) *Elsevier, Boston*, Chapter 5, pp. 85–113.

Palacz, Z. and Saunders, A. D. (1986) Coupled trace element and isotope enrichment on the Cook-Austral-Samoa Islands, southwest Pacific. *Earth Planet. Sci. Lett.* **79**, 270-280.

Patchett, P.J. and Tatsumoto, M. (1980) Hafnium isotope variations in oceanic basalts. *Geophys. Res. Lett.* **7**, 1077-1080.

Pietsch, R., and Uenzelmann-Neben, G. (2015) The Manihiki Plateau—A multistage volcanic emplacement history, *Geochem. Geophys. Geosyst.* **16**, 2480–2498, doi:10.1002/2015GC005852.

Pringle, M. S. and Dalrymple, G. B. (1993) Geochronological constraints on a possible hot spot origin for Hess Rise and the Wentworth Seamount Chain. In *The Mesozoic Pacific: Geology, Tectonics, and Volcanism* (eds. M. S. Pringle, W. W. Sager, W. V. Sliter, and S. Stein). *Am. Geophys. Union Geophys. Monogr.* **77**, pp. 263-277.

Richards, M. A., Duncan, R. A. and Courtillot, V. E. (1989) Flood basalts and hot-spot tracks: plume heads and tails. *Science* **246**, 103-107.

Rohde, J. K., van den Bogaard, P., Hoernle, K., Hauff, F. and Werner, R. (2013) Evidence for an age progression along the Tristan-Gough volcanic track from new $^{40}Ar/^{39}Ar$ ages on phenocryst phases. *Tectonophys*. **604**, 60-71.

Sager, W. W. (2005) What built Shatsky Rise, a mantle plume or ridge tectonics? In *Plates, plumes, and paradigms* (eds. G. R. Foulger, J. H. Natland, D. C. Presnall, and D. L. Anderson) *Geol. Soc. Am. Spec. Paper* **388** pp. 721-733.

Sager, W. W. (2007) Divergence between paleomagnetic and hotspot model predicted polar wander for the Pacific plate with implication for hotspot fixity. In *Plates, plumes, and planetary processes* (eds. G. R. Foulger and D. M. Jurdy) *Geol. Soc. Am. Spec. Paper* **430** pp. 335-359.

Sager, W. W. and Han, H-C. (1993) Rapid formation of the Shatsky Rise oceanic plateau inferred from its magnetic anomaly. *Nature* **364**, 610-613.

Sager, W. W. and Keating, B. H. (1984) Paleomagnetism of Line Islands Seamounts: Evidence for Late Cretaceous and Early Tertiary volcanism. *J. Geophys. Res.* **89**, 11135-11151.

Sager, W. W., Klaus, A., Nakanishi, M., Brown, G. R., and Khankishieva, L. M. (1995) Shatsky Rise expedition: R/V Thomas G. Thompson Cruise TN037. *Technical Report 95-5-T*, Texas A&M University, 95pp.

Sager, W. W., Kim, J., Klaus, A., Nakanishi, M. and Khankishieva, L. M. (1999) Bathymetry of Shatsky Rise, northwest Pacific Ocean: Implications for ocean plateau development at a triple junction. *J. Geophys. Res.* **104**, 7557-7576.

Sager, W.W., Sano, T., Geldmacher, J., and the IODP Expedition 324 Scientists (2011) IODP Expedition 324: ocean drilling at Shatsky Rise gives clues about oceanic plateau formation. *Sci. Drill.,* **12,** 24–31.doi:10.2204/iodp.sd.12.03.2011.

Sager, W. W., Zhang, J., Korenaga, J., Sano, T., Koppers, A. A . P., Widdowson, M., Mahoney, J. J. (2013) An immense shield volcano within the Shatsky Rise oceanic plateau, northwest Pacific Ocean. *Nat. Geosci.* **6,** 976–981. doi:10.1038/ngeo1934

Sager, W. W., Pueringer, M., Carvallo, C., Ooga, M., Housen, B. and Tominaga, M. (2015) Paleomagnetism of igneous rocks from the Shatsky Rise: Implications for paleolatitude and oceanic plateau volcanism. In *The Origin, Evolution, and Environmental Impact of Oceanic Large Igneous Provinces* (eds. C. R. Neal, W. W. Sager, T. Sano and E. Erba). Special Paper 511 (8), Geological Society of America Special Paper 511, p. 147-171.

Sano, T., Shimizu, K., Ishikawa, A., Senda, R., Chang, Q., Kimura, J-I., Widowson, M., and Sager, W. W. (2012) Variety and origin of magmas on Shatsky Rise, northwest Pacific Ocean. Geochem. Geophys. Geosyst. 13, Q08010, doi:10.1029/2012GC004235.

Schiano, P., Birck, J.-L. and Allegre, C.J. (1997) Osmium-strontium-neodymium-lead isotopic variations in mid-ocean ridge basalt glasses and the heterogeneity of the upper mantle. *Earth Planet. Sci. Lett.* **150**, 363-379.

Scott, R. B. (1981) Geochemistry of igneous rocks in Deep Sea Drilling Project Hole 465A, Hess Rise: Significance to oceanic plateau petrology and evolution, Deep Sea Drilling Project Leg 62. In *Deep-Sea Drilling Project Initial Reports 62* (eds. J. Thiede, T. L. Vallier, L. et al.). U. S. Govt. Printing Office, Washington. pp. 955-960.

Seifert, K. E., Vallier, T. L., Windom, K. E. and Morgan, S. R. (1981) Geochemistry and petrology of igneous rocks, Deep Sea Drilling Project Leg 62. In *Deep-Sea Drilling Project Initial Reports 62* (eds. Thiede, J., Vallier, T. L. et al.). U. S. Govt. Printing Office, Washington. pp. 945-953.

Shimizu, K. Sano, T., Tejada, M. L. G., Hyodo, H., Sato, K., Suzuki, K., Chang, Q. and Nakanishi, M. (2015) Alkalic magmatism in the Lyra Basin: A missing link in the late stage evolution of the Ontong Java Plateau. In *The Origin, Evolution, and Environmental Impact of Oceanic Large Igneous Provinces* (eds. C. R. Neal, W. W. Sager, T. Sano and E. Erba). Special Paper 511 (13), Geological Society of America Special Paper 511, p. 233-249.

Shimoda, G., Ishizuka, O., Yamashita, K., Yoshitake, M., Ogasawara, M. and Yuasa, M. (2011) Tectonic influence on chemical composition of ocean island basalts in the West and South Pacific: Implications for a deep mantle origin. *Geochem. Geophys. Geosys.* **12,** Q07020, doi:10.1029/ 2011GC003531.

Sikora, P. J. and Bergen, J. A. (2004) Lower Cretaceous planktonic foraminiferal and nannofossil biostratigraphy of Ontong Java Plateau sites from DSDP Leg 30 and ODP Leg 192. In *Origin and Evolution of the Ontong Java Plateau* (eds. J. G. Fitton, J. J. Mahoney, P. J. Wallace and A. D. Saunders) Geological Society of London Special Publication 229, p. 83-111.

Staudigel, H., Park, K-H., Pringle, M., Rubenstone, J. L., Smith, W.H. F. and Zindler, A. (1991) The longevity of the South Pacific isotopic and thermal anomaly. *Earth Planet. Sci. Lett.* **102**, 24-44.

Steiger, R.H. and Jäger, E. (1977) Subcommission on geochronology: Convention on the use of decay constants in geo- and cosmochronology. *Earth and Planetary Science Letters* **36**, 359–362, doi: 10.1016/0012-821X(77)90060-7.

Tatsumi, Y., Shinjoe, H., Ishizuka, H., Sager, W. and Klaus, A. (1998) Geochemical evidence for a mid-Cretaceous superplume. *Geology* **26**, 151-154.

Taylor, B. (2006) The single largest oceanic plateau: Ontong Java-Manihiki-Hikurangi. *Earth Planet. Sci. Lett.* **241**, p. 372-380.

Tejada, M. L. G. (1998) Geochemical studies of Pacific oceanic plateaus: The Ontong Java Plateau and Shatsky Rise. Ph. D. Thesis, University of Hawaii.

Tejada, M. L. G., Mahoney, J. J., Duncan, R. A. and Hawkins, M. P. (1996) Age and geochemistry of basement and alkalic rocks of Malaita and Santa Isabel, Solomon Islands, southern margin of Ontong Java Plateau. *J. Petrol.* **37**, 361-394.

Tejada, M. L. G., Mahoney, J. J., Tatsumi, Y. and Sager, W. W. (2001) Water-rock interaction in dredged lavas from Shatsky Rise, Pacific Ocean. In *Water-rock Interaction* (ed. Cidu, R.) Proceedings of the Tenth International Symposium on Water-Rock Interaction **2**, 935-938.

Tejada, M. L. G., Mahoney, J. J., Neal, C. R., Duncan, R. A. and Petterson, M. G. (2002) Basement geochemistry and geochronology of Central Malaita, Solomon Islands, with implications for the origin and evolution of the Ontong Java Plateau. *J. Petrol.* **43,** 449-484.

Tejada, M. L. G., Mahoney, J. J., Castillo, P. R., Ingle, S. P., Sheth, H. C., and Weis, D. (2004) Pin-pricking the elephant: Evidence on the origin of the Ontong Java Plateau from Pb-Sr-Hf-Nd isotopic characteristics of ODP Leg 192 basalts. In *Origin and Evolution of the Ontong Java Plateau* (eds. J. G. Fitton, J. J. Mahoney, P. J. Wallace and A. D. Saunders) Geological Society of London Special Publication 229, p. 133-150.

Tejada, M. L. G., Suzuki, K., Hanyu, T., Mahoney, J. J., Ishikawa, A., Tatsumi, Y., Chang, Q. and Nakai, S. (2013) Cryptic lower crustal signature in the source of the Ontong Java Plateau revealed by Os and Hf isotopes. *Earth Planet. Sci. Lett.* **377-378**, 84-96.

Tejada, M. L. G., Hanyu, T., Ishikawa, A., Senda, R., Suzuki, K., Fitton, G. and Williams R. (2015a) Re-Os isotope and platinum group elements of a FOcal ZOne mantle source, Louisville Seamounts Chain, Pacific ocean, *Geochem. Geophys. Geosyst.* **16**, 486–504, doi:10.1002/2014GC005629.

Tejada, M. L. G., Shimizu, K., Suzuki, K., Hanyu, T., Sano, T., Nakanishi, M., Nakai, S., Ishikawa, A., Chang, Q., Miyazaki, T, Hirahara, Y., Takahashi, T. and Senda, R. (2015b) Isotopic evidence for a link between the Lyra Basin and Ontong Java Plateau. In *The Origin, Evolution, and Environmental Impact of Oceanic Large Igneous Provinces* (eds. C. R. Neal, W. W. Sager, T. Sano and E. Erba). Special Paper 511 (14), Geological Society of America Special Paper 511, p. 251-269.

Thiede, J., Vallier, T. L., and Adelseck, C. G. (1981) Deep Sea Drilling Project Leg 62, North Central Pacific Ocean: Introduction, cruise narrative, principal results, and explanatory notes. In *Deep-Sea Drilling Project Initial Reports 62* (eds. Thiede, J., Vallier, T. L. et al.). U. S. Govt. Printing Office, Washington. pp. 5-31.

Thompson, P. M. E., Kempton, P. and Kerr, A. C. (2008) Evaluation of the effects of alteration and leaching on Sm-Nd and Lu-Hf systematics in submarine mafic rocks. *Lithos* **104,** 164-176.

Timm, C., Hoernle, K., Werner, R., Hauff, F., van den Bogaard, P., Michael, P., Coffin, M.F. and Koppers, A. (2011) Age and geochemistry of the oceanic Manihiki Plateau, SW Pacific: New evidence for a plume origin. *Earth Planet. Sci. Lett.* **304,** 135-146.

Todt, W., Cliff, R. A., Hanser, A. and Hoffman, A. W. (1996) Evaluation of ^{202}Pb - ^{205}Pb double spike for high-precision lead isotope analysis. In *Earth Processes: Reading the Isotopic Code* (eds. A. Basu and S. Hart). *Geophysical Monograph* **95**, *American Geophysical Union*, p. 429-437.

Vallier, T. L., Windom, K. E., Siefert, K. E. and Thiede, J. (1980) Volcanic rocks cored on Hess Rise, western Pacific Ocean. *Nature* **286**, 48-50.

Vallier, T. L., Dean, W. E., Rea, D. K. and Thiede, J. (1983) Geological evolution of Hess Rise, central north Pacific Ocean. *Geol. Soc. Am. Bull.* **94**, 1289-1307.

Vanderkluysen, L., Mahoney, J. J., Koppers, A. A. P., Beier, C., Regelous, M., Gee, J. S. and Lonsdale, P. F. (2014) Louisville Seamount Chain: Petrogenetic processes and geochemical evolution of the mantle source. *Geochem. Geophys. Geosyst.* **15**, doi:10.1002/2014GC005288.

Van Keken, P. E., King, S. D., Schmeling, H., Christensen, U. R., Neumeister, D. and Doin, M.-P. (1997) A comparison of methods for the modeling of thermochemical convection. *J. Geophys. Res.* **102**, 22477-22495.

Vidal, P., Chauvel, C. and Brousse, R. (1984) Large mantle heterogeneity beneath French Polynesia. *Nature* **307**, 536-538.

Wheat, C. G., Feely, R. A. and Mottl, M. J. (1996) Phosphate removal by oceanic hydrothermal processes: An update of the phosphorous budget in the oceans, *Geochim. Cosmochim. Acta* **60**, 3593-3608.

White, W. M. (1993) $^{238}U/^{204}Pb$ in MORB and open system evolution of the depleted mantle. *Earth Planet. Sci. Lett.* **115**, 211-226.

White, W. M., Hoffman, A. W. and Puchelt, H. (1987) Isotope geochemistry of Pacific mid-ocean ridge basalts. *J. Geophys. Res.* **92**, 4881-4893.

Williams, R., Hamelin, C., Geldmacher, J., Mahoney, J. J., Barry, T. L. and Saunders, A. D. (2014) Isotope geochemistry of Nd, Hf, Sr and Pb in lavas of the Louisville Seamount Trail: nature of the mantle source. Abstract, VMSG Annual Meeting, Edinburgh. http://dx.doi.org/10.6084/m9.figshare.1506807

Windom, K. E., Seifert, K. E., Vallier, T. L. (1981) Igneous evolution of Hess Rise: Petrologic evidence from DSDP Leg 62. *J. Geophys. Res.* **86,** 6311-6322.

Zhang, J., Sager, W. W. and Korenaga, J. (2015) The Shatsky Rise oceanic plateau structure from two-dimensional multichannel seismic reflection profiles and implications for oceanic plateau formation. In *The Origin, Evolution, and Environmental Impact of Oceanic Large Igneous Provinces* (eds. C. R. Neal, W. W. Sager, T. Sano and E. Erba). Special Paper 511 (6), Geological Society of America Special Paper 511, p. 103-126.

Table 1

Table 1. Dredge locations (from Sager et al., 1995) of TN037 dredges and drill sites on Hess Rise that recovered basement rocks.

Dredge No.	Geographic Location Lat° N	Lon° E	Seafloor Age	Locality	Previous Age Data, Ma	Water Depth, m
D1	36° 27.02'	169° 18.13'	129-125 Ma (M3-M0)	East Ojin Rise Seamounts, Seamount 6		4267
D2	37° 37.58'	165° 27.52'	135-131 Ma (M10-M5)	West Ojin Rise Seamounts, Victoria Seamount		4833
D4	39° 50.26'	163° 54.79'	135-131 Ma (M10-M5)	Shatsky Rise North flank, Earthwatch Seamount		4000
D9	36° 31.15'	159° 11.62'	142-139 Ma (M16-M14)	Shatsky Rise ORI Massif, East side of summit	134±1[a]	3900
D11	35° 15.70'	158° 57.05'	144-142 Ma (M18-M16)	Cooperation Seamount		3760
D13	32° 39.97'	158° 03.79'	150-144 Ma (M21-M18)	Shatsky Rise, TAMU Massif East side, Toronto Ridge	133.9±2.3[b] 143.1±3.3[b] 144.4±1.0 (n=4)[b]	2357
D14	32° 39.97'	158° 03.79'	150-144 Ma (M21-M18)	Shatsky Rise, TAMU Massif West side, Toronto Ridge	144.6±0.8[c] 143.7±3.0[d] 144.8±1.2[d]	2155
Hess Rise						
DSDP Site 464	39° 51.64’	173° 53.33’		Northwest extension	~113	4637
DSDP Site 465A	33° 49.23’	178° 55.14’		High crest, southern end	~100-98; >90-94[e]	2161

Notes: Assigned seafloor ages for seafloor magnetic anomalies (Nakanishi et al., 1999) are based on geologic time scale of Ogg (2012). Previous age data are from biostratigraphy (Thiede et al., 1981) and ^{40}Ar-^{39}Ar dating on Hess and Shatsky (TAMU and ORI) rises: a) Heaton and Koppers, 2014; b) Geldmacher et al., 2014; c) Mahoney et al., 2005; d) Koppers, 2010; e) Pringle and Dalrymple, 1993.

Table 2

Table 2. ICP-MS trace element concentrations (ppm).

	Rb	Ba	Th	U	Nb	Ta	La	Ce	Pb	Pr	Sr	Nd	Sm	Zr	Hf	Eu	Gd	Tb	Dy	Y	Ho	Er	Tm	Yb	Lu	Sc	Co	Ni	Cu
East Ojin Rise Seamounts, Seamount 6																													
TN037 D1-05	46.1	72.7	1.16	0.49	13.1	0.86	29.5	30.4	0.37	6.03	256	27.0	6.23	153	4.11	2.06	7.34	1.13	6.83	45.2	1.41	3.98	0.54	3.33	0.51	39.8	17.0	23.3	177
TN037 D1-08	50.5	84.7	1.29	0.80	16.3	1.03	23.9	36.3	0.84	5.69	329	26.0	6.42	177	4.66	2.09	6.98	1.13	6.64	38.9	1.34	3.81	0.53	3.30	0.50	42.3	14.2	23.0	150
TN037 D1-10	26.0	49.2	1.09	0.68	10.9	0.78	72.7	26.8	0.62	13.2	257	58.9	12.5	100	3.14	3.65	15.8	2.30	13.9	113	2.97	8.59	1.17	7.39	1.17	51.3	10.3	24.4	117
TN037 D1-12	45.8	83.4	1.33	0.50	15.7	1.03	49.0	35.2	2.27	10.9	338	48.4	10.5	177	4.77	3.19	12.4	1.84	10.9	76.7	2.25	6.31	0.84	5.10	0.77	35.6	15.4	16.6	122
TN037 D1-13	42.5	68.0	1.10	0.68	13.0	0.83	68.0	31.9	0.58	8.65	331	37.4	7.56	148	3.85	2.42	10.0	1.44	8.88	85.1	1.97	5.65	0.75	4.64	0.73	34.8	18.8	31.3	165
TN037 D1-16	50.4	85.8	1.48	0.67	16.8	1.16	54.2	32.4	1.05	11.5	339	50.2	10.4	172	5.16	3.08	11.7	1.70	9.79	68.7	1.99	5.62	0.75	4.63	0.68	38.9	12.6	15.4	127
Shatsky Rise, North Flank [Earthwatch Seamount]																													
TN037 D4-01	45.3	89.8	1.36	1.87	16.7	1.07	112	35.0	3.13	19.4	305	85.6	17.5	193	4.98	5.02	23.5	3.43	21.2	195	4.74	13.8	1.84	11.3	1.76	38.2	14.1	24.7	131
TN037 D4-05	57.4	77.6	1.37	1.41	14.8	0.99	28.7	32.8	0.85	5.95	323	27.2	6.60	171	4.55	2.24	8.28	1.34	8.38	57.9	1.78	5.25	0.73	4.62	0.72	43.4	12.1	16.7	91.9
TN037 D4-11	46.0	85.9	1.32	1.59	15.5	1.04	47.7	32.7	0.83	6.67	302	30.1	7.03	179	4.76	2.35	9.05	1.46	9.39	86.9	2.13	6.47	0.93	6.03	0.99	35.2	14.0	20.2	125
TN037 D4-12	53.9	59.7	0.93	1.21	11.2	0.75	71.7	24.6	0.73	10.3	258	45.1	9.09	130	3.43	2.73	12.7	1.86	11.7	112	2.63	7.69	1.03	6.33	0.99	38.3	9.79	16.7	106
TN037 D4-13	45.5	66.3	1.11	1.08	12.3	0.81	26.4	26.7	0.93	6.64	272	30.1	7.29	133	3.69	2.29	8.92	1.40	8.52	54.2	1.78	5.10	0.71	4.52	0.70	37.2	11.3	14.5	74.9
Shatsky Rise, Cooperation Seamount																													
TN037 D11-01	53.8	529	6.44	1.47	67.7	4.36	48.1	90.5	2.57	10.6	759	40.5	7.55	282	6.55	2.38	6.63	1.01	5.49	26.7	1.05	2.92	0.39	2.43	0.36	25.6	26.4	93.7	51.6
TN037 D11-04	90.8	651	7.85	1.89	81.5	5.30	56.8	107	3.84	12.0	591	44.3	7.94	344	7.73	2.49	6.74	1.03	5.58	28.0	1.08	3.07	0.43	2.74	0.43	23.2	38.9	105	13.3
TN037 D11-05	57.0	623	6.31	1.20	66.5	4.40	52.5	93.3	3.06	11.2	514	43.1	8.03	276	6.59	2.46	7.22	1.09	6.01	32.2	1.17	3.27	0.45	2.83	0.42	26.6	30.8	64.8	38.2
Hess Rise																													
464, 34-CC, 10-16	9.69	116	0.35	0.14	4.5	0.29	4.9	13.0	0.47	2.1	138	10.6	3.25	112	2.76	1.20	3.64	0.64	4.09	20.8	0.83	2.33	0.35	2.27	0.33				
465, 45-1, 99-102	55.4	587	7.60	1.14	112	6.29	60.3	96	5.31	13.7	178	49.2	8.02	701	13.8	2.38	6.35	0.94	5.19	27.7	1.00	2.80	0.42	2.85	0.44				
465, 45-2, 113-116	48.4	611	8.20	1.64	113	6.28	60.9	114.7	5.72	14.3	199	52.5	9.03	933	16.1	2.61	7.37	1.13	6.51	35.9	1.28	3.63	0.56	3.86	0.62				
BHVO-2,																													
JAMSTEC	9.46	138	1.24	0.43	17.9	1.17	15.3	37.9	1.46	5.37	411	24.8	6.24	177	4.76	2.10	6.39	0.99	5.45	24.3	1.02	2.65	0.35	2.06	0.29	30.3	45.1	125	134
IGUK	9.33	131	1.23	0.42	17.9	1.08	15.4	37.7	1.81	5.32	385	25	6.24	174	4.25	2.12	6.18	0.95	5.41	25.5	1	2.5	0.33	2	0.29	31.4	44.8	119	133
GEOREM	9.11	131	1.22	0.40	18.1	1.14	15.2	37.5	1.6	5.35	396	24.5	6.07	172	4.36	2.07	6.24	0.92	5.31	26	0.98	2.5	0.33	2.00	0.27	32.0	45.0	119	127
	0.04	1	0.06	<0.01	0.1	0.60	0.01	0.2	0.3	0.17	1	0.01	0.01	11	0.14	0.02	0.03	0.03	0.02	2	<0.01	0	<0.01	0	0.01	0.10	0.3	1	7

Notes: ICPMS data for Ojin Rise, Earthwatch, and Cooperation seamounts were obtained at JAMSTEC. ICPMS measurement for Hess Rise was conducted at Institute of Geosciences, University of Kiel (IGUK)

GEOREM = GeoReM preferred values (http://georem.mpch-mainz.gwdg.de/)

Table 3

Table 3. Age-corrected Nd, Hf, and Pb isotope data and isotope dilution parent-daughter element concentrations (in ppm).

Sample No.	$(^{143}Nd/^{144}Nd)_t$	$\varepsilon_{Nd}(t)$	$(^{176}Hf/^{177}Hf)_t$	$\varepsilon_{Hf}(t)$	$(^{206}Pb/^{204}Pb)_t$	$(^{207}Pb/^{204}Pb)_t$	$(^{208}Pb/^{204}Pb)_t$	Sm	Nd	Th	U	Pb
East Ojin Rise Seamounts, Seamount 6 (t ≈ 120 Ma)												
TN037-D1-05 *	0.512822	6.8	0.282969	9.3	18.87	15.58	38.86					
TN037-D1-08 *	0.512900	8.3	0.282989	10.0	18.67	15.55	38.65					
TN037-D1-12 #	0.512983	9.9			18.71	15.56	38.69	0.1429	0.8432	0.0205	0.118	0.520
duplicate	0.513003	10.3			18.59	15.54	38.78	0.1391	0.8109	0.0210	0.113	0.283
average	0.512993	10.1			18.65	15.55	38.74					
West Ojin Rise Seamounts, Seamount 8 [North Victoria Seamount] (t ≈ 120 Ma)												
TN037-D2-01 †	0.512834	7.0			18.32	15.54	38.18	0.2489	1.071	0.0266	0.252	0.561
Shatsky Rise, North Flank [Earthwatch Seamount] (t ≈ 120 Ma)												
TN037-D4-05 *	0.512728	4.9			18.17	15.56	38.14					
TN037-D4-12 *			0.282939	8.2	17.95	15.55	37.99					
TN037-D4-13 †	0.512685	4.1	0.282981	9.7	18.09	15.55	38.12	1.594	6.942	0.315	0.497	0.570
TN037-D4-13 #	0.512751	5.4										
Shatsky Rise, Cooperation Seamount (t ≈ 122 Ma)												
TN037-D11-01 †	0.512864	7.6	0.283037	11.7	19.09	15.55	38.72	2.930	16.12	3.090	1.130	3.377
TN037-D11-01 #	0.512922	8.7			19.04	15.54	38.76					
TN037-D11-05 *	0.512863	7.6	0.283033	11.6	19.05	15.54	39.02					
TN037-D11-04 *	0.512849	7.3			19.04	15.54	38.85					
Shatsky Rise, Toronto Ridge (t ≈ 129 Ma)												
TN037-D14-01 †[b]	0.512971	9.9			18.17	15.45	37.74	2.136	9.576	0.669	0.277	1.277

Table 3. Age-corrected Nd, Hf, and Pb isotope data and isotope dilution parent-daughter element concentrations (cont'd).

Sample No.	(143Nd/144 Nd)$_t$	$\varepsilon_{Nd}(t)$	$(^{176}Hf/^{177}Hf)_t$	$\varepsilon_{Hf}(t)$	$(^{206}Pb/^{204}Pb)_t$	$(^{207}Pb/^{204}Pb)_t$	$(^{208}Pb/^{204}Pb)_t$	Sm	Nd	Th	U	Pb
Northern Hess Rise (t ≈ 110 Ma)												
464-34R-CC † [a]	0.512913	8.3						2.975	9.875			
464-34R-CC #[b]	0.512946	8.9			18.15	15.48	37.86	0.3175	0.8661	0.141	0.105	0.252
464-34R-CC (10-16) *	0.512935	8.7	0.283124	14.5	18.29	15.49	37.96					
duplicate	0.512951	9.0			18.29	15.50	37.96					
average	0.512943	8.9			18.29	15.50	37.96					
Southern Hess Rise (t ≈ 110 Ma)												
465A-42R-2 (76-78) † [a]	0.512782	5.7						10.94	68.7			
465A-42R-2 (76-78) #	0.512772	5.5			19.07	15.59	39.41	3.645	19.21	3.097	1.326	3.268
465A-45R-1 (99-102) *	0.512795	6.0	0.282905	6.8	19.05	15.60	39.33					
465A-45R-2 (113-116) *	0.512801	6.1	0.282906	6.8	19.00	15.60	39.24					

Notes:
Data are reported relative to standard values for La Jolla Nd of $^{143}Nd/^{144}Nd$ = 0.511850; for JMC 475, $^{176}Hf/^{177}Hf$ = 0.282163. The total range measured for La Jolla Nd is 0.000008 (0.2 ε units); for JMC 475-calibrated in-house SPEX monitor, it is 0.000006 over the measurement period. Pb isotope ratios are reported relative to NBS 981 standard values of Todt et al. (1996); the total ranges measured are 0.012 for $^{206}Pb/^{204}Pb$, 0.012 for $^{207}Pb/^{204}Pb$, and 0.038 for $^{208}Pb/^{204}Pb$. Isotopic fractionation corrections are described in Appendix I and age-correction used the isotope dilution data for the parent-daughter ratios, except for Hf data, which used ICPMS values. ε_{Nd}= 0 today corresponds to $^{143}Nd/^{144}Nd$ = 0.51263; for $^{147}Sm/^{144}Nd$ = 0.1960 (Bouvier et al., 2008), $\varepsilon_{Nd}(t)$ = 0 corresponds to $^{143}Nd/^{144}Nd$ = 0.512465 at 129 Ma, 0.512474 at 122 Ma, 0.512476 at 120 Ma, and 0.512489 at 110 Ma. Within-run errors on the isotopic data above are less than or equal to the external uncertainties on these standards. Estimated uncertainties on isotope dilution abundances are <0.2% on Sm and Nd, <2 % on Th, <1 % on U, and < 1% on Pb. Total blanks are negligible: <15 picograms for Nd and <20 picograms for Hf, <5 picograms for U, <3 pg for Th, and 5-30 picograms for Pb. Duplicate analyses were made on separate dissolutions of powder from re-picked chips of the same sample.

a: from Mahoney, 1987

b: from Mahoney et al., 2005

* handpicked chips cleaned in 2N HCl at 70°C for one hour followed by triple rinse in ultrapure water at GEOMAR

† handpicked chips cleaned at room temperature for 5 min each in MQ water with a few drops of HF-HNO3 mixture added, followed by 6N HCl and then rinsed in ultrapure water and powdered before digestion at UH

splits of powders† but further leached ultrasonically with 6N HCl at room temperature for 5min, repeated until solution is clear and almost colorless at UH (Mahoney, 1987; Nobre Silva et al., 2009).

Table 4

Sample Information					Plateau							Normal Isochron			Inverse Isochron			Total Fusion	
Experiment Number	Sample ID	Dredge Loc. Lat.	Lon.	Material	Age Type	Age ± 2σ [Ma]	^{39}Ar [%]	K/Ca ± 2σ	MSWD	n	N	Age ± 2σ [Ma]	$^{40}Ar/^{36}Ar$ ± 2σ intercept	MSWD	Age ± 2σ [Ma]	$^{40}Ar/^{36}Ar$ ± 2σ intercept	MSWD	Age ± 2σ [Ma]	K/Ca ± 2σ
East Ori Massif																			
13D04739	TN037 D09-04	36.52	159.19	Groundmass	No Age						23							98.74 ± 0.16	0.047 ± 0.000
Cooperation Seamount																			
13D03297	TN037 D11-01	35.26	158.95	Groundmass	No Age						34							122.69 ± 0.19	0.375 ± 0.001
13D04771	TN037 D11-05	35.26	158.95	Groundmass	Minimum Age	122.46 ± 0.27	19.16	0.779 ± 0.04	9.31	10	44	122.24 ± 0.40	301.13 ± 13.47	12.79	122.47 ± 0.36	294.90 ± 12.14	10.45	110.44 ± 0.16	0.309 ± 0.001
Toronto Ridige, Shatsky Rise																			
13D05465	TN037 D13-02	32.72	158.25	Plagioclase	Eruption Age	129.42 ± 0.32	94.64	0.004 ± 0.00	0.82	12	19	129.20 ± 0.55	309.81 ± 40.44	0.92	129.29 ± 0.54	307.07 ± 39.62	0.87	129.44 ± 0.34	0.004 ± 0.000
13D03726	TN037 D14-1A	32.67	158.06	Plagioclase	Minimum Age	120.78 ± 0.44	30.72	0.004 ± 0.00	0.51	4	24	122.53 ± 2.93	195.22 ± 165.44	0.48	122.20 ± 3.02	214.24 ± 167.13	0.45	119.70 ± 0.31	0.004 ± 0.000
13D04924	TN037 D14-1B	32.67	158.06	Plagioclase	No Age						22							111.30 ± 0.41	0.004 ± 0.000

Figure 1

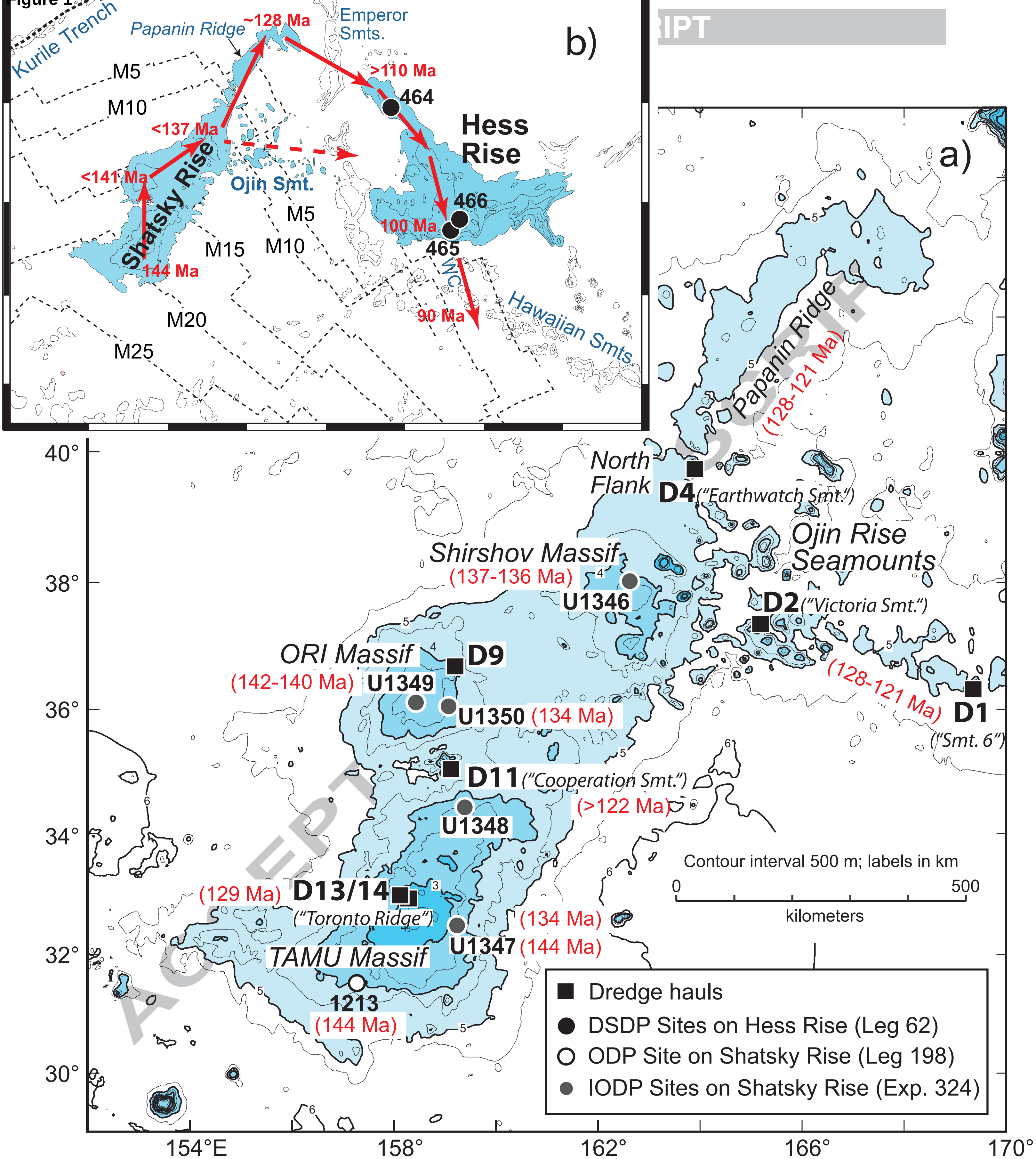

Figure 1

Figure 2

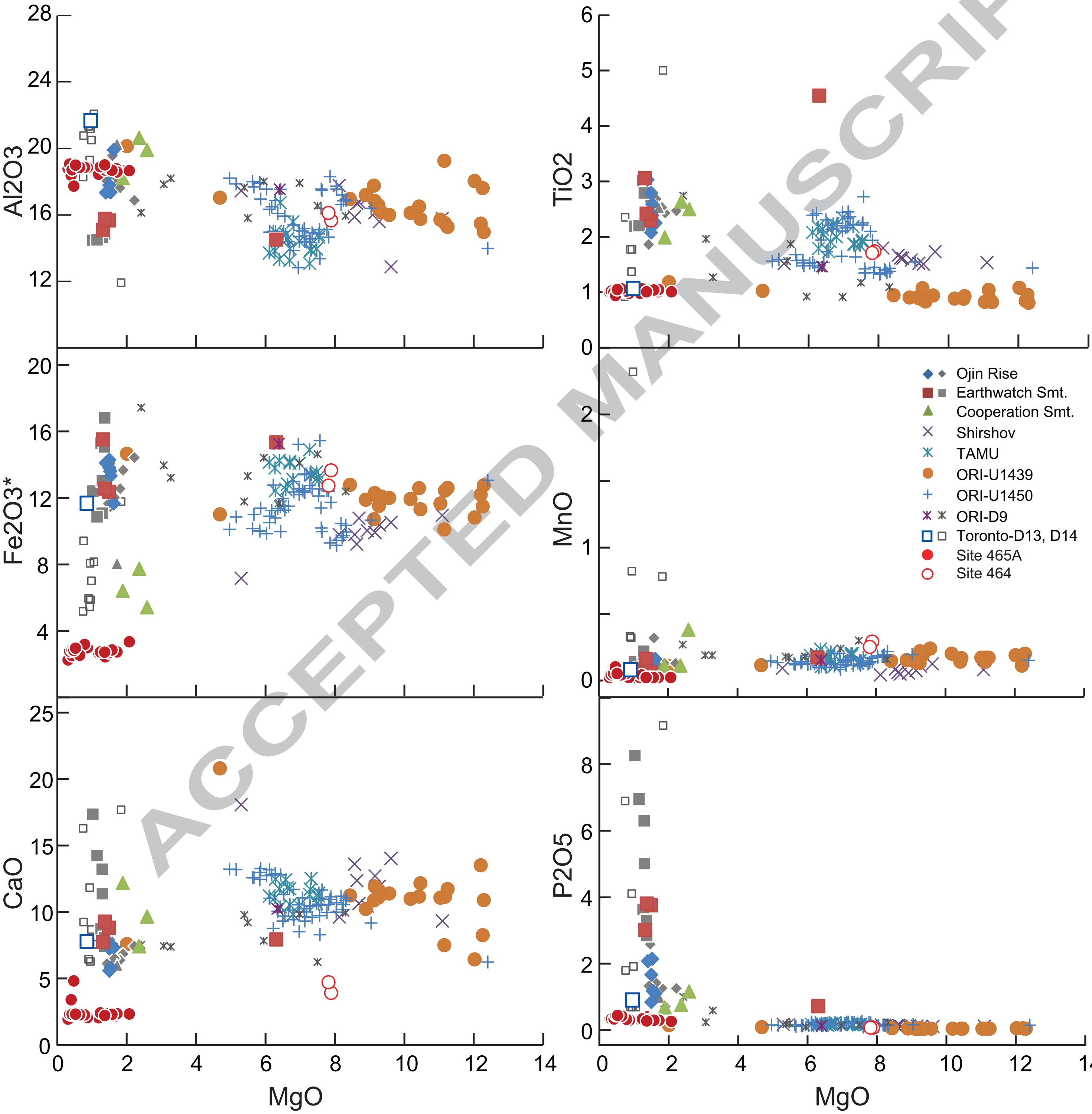

Figure 2

Figure 3

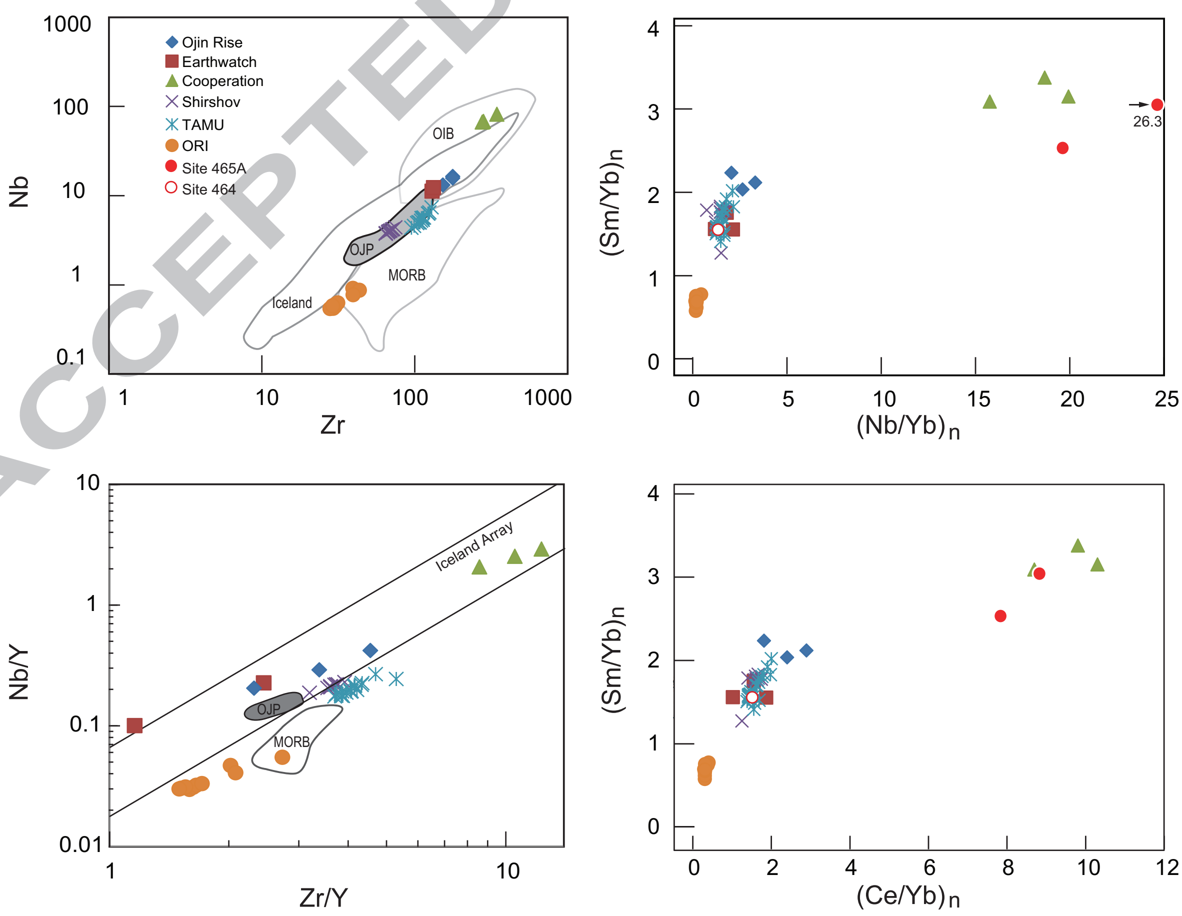

Figure 3

Figure 4

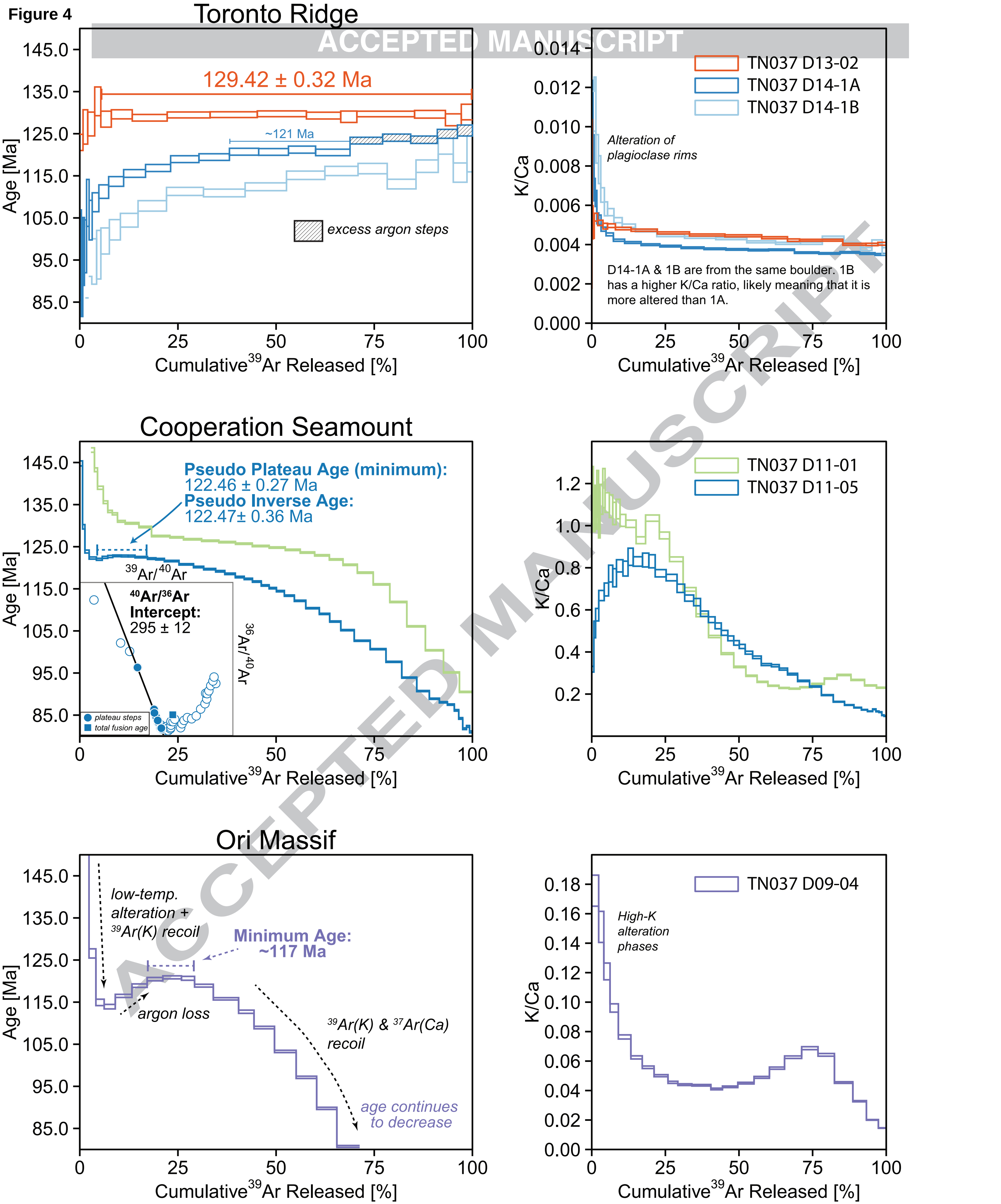

Figure 4

Figure 5

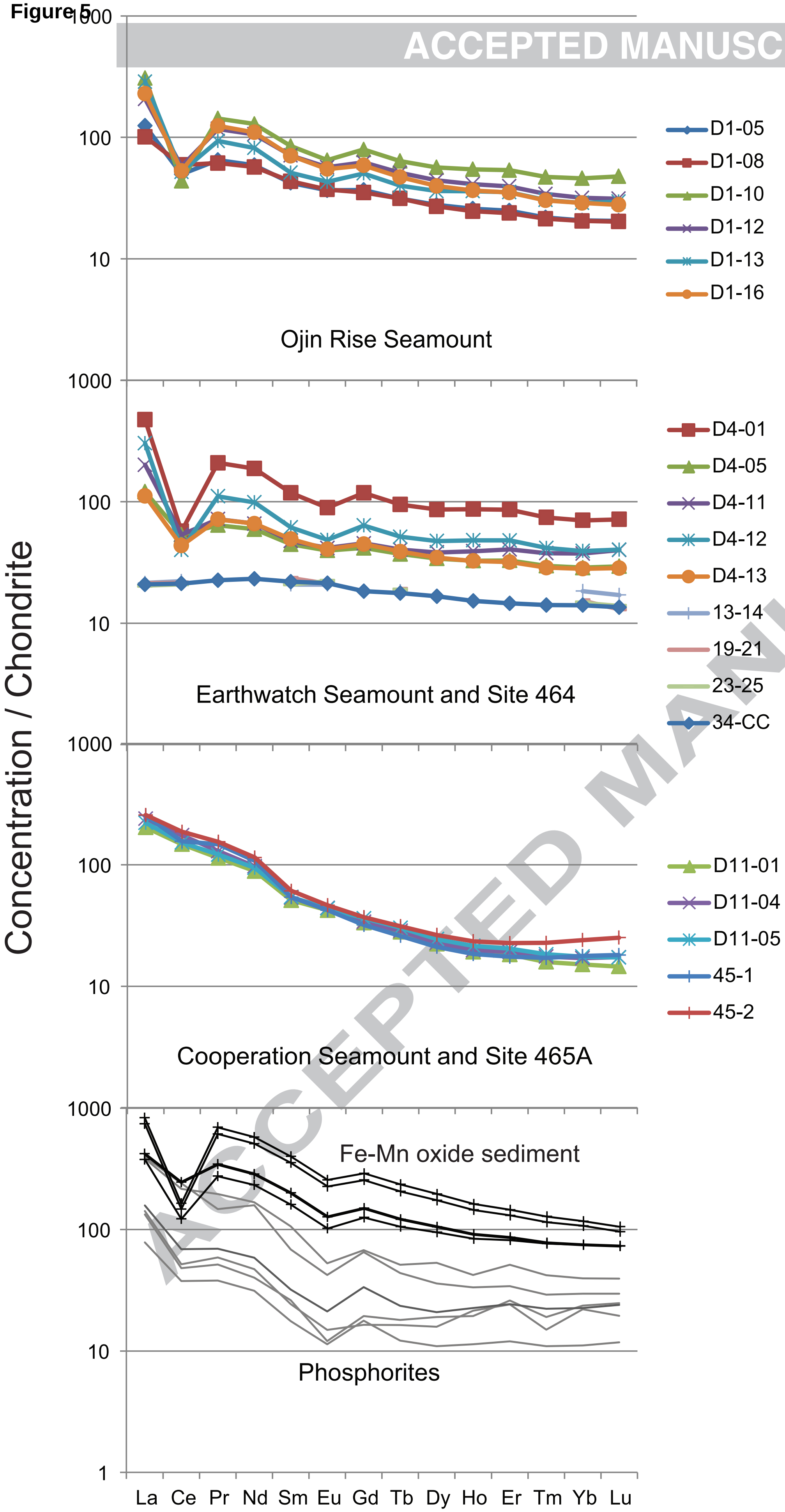

Figure 5

Figure 6

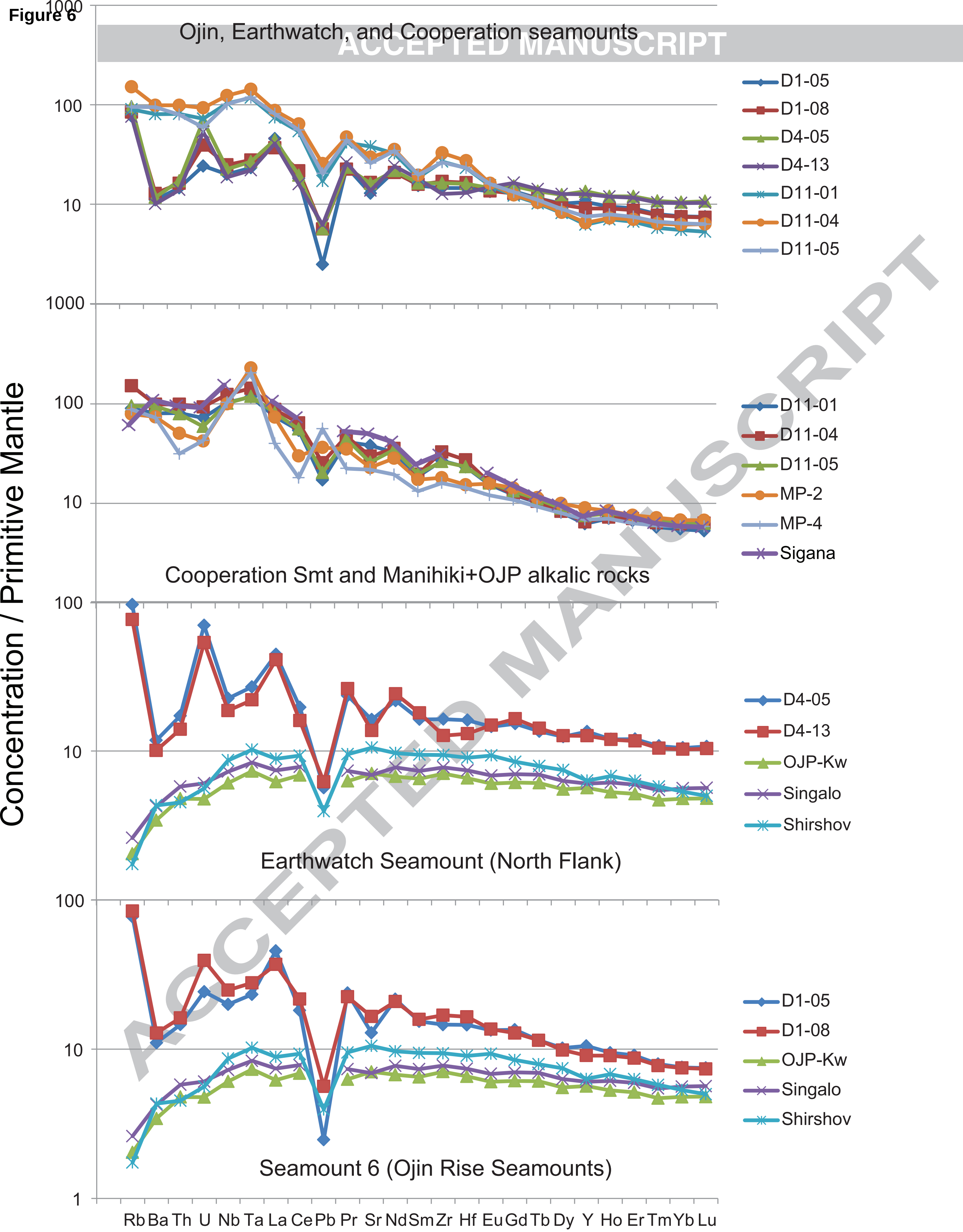

Figure 6

Figure 7

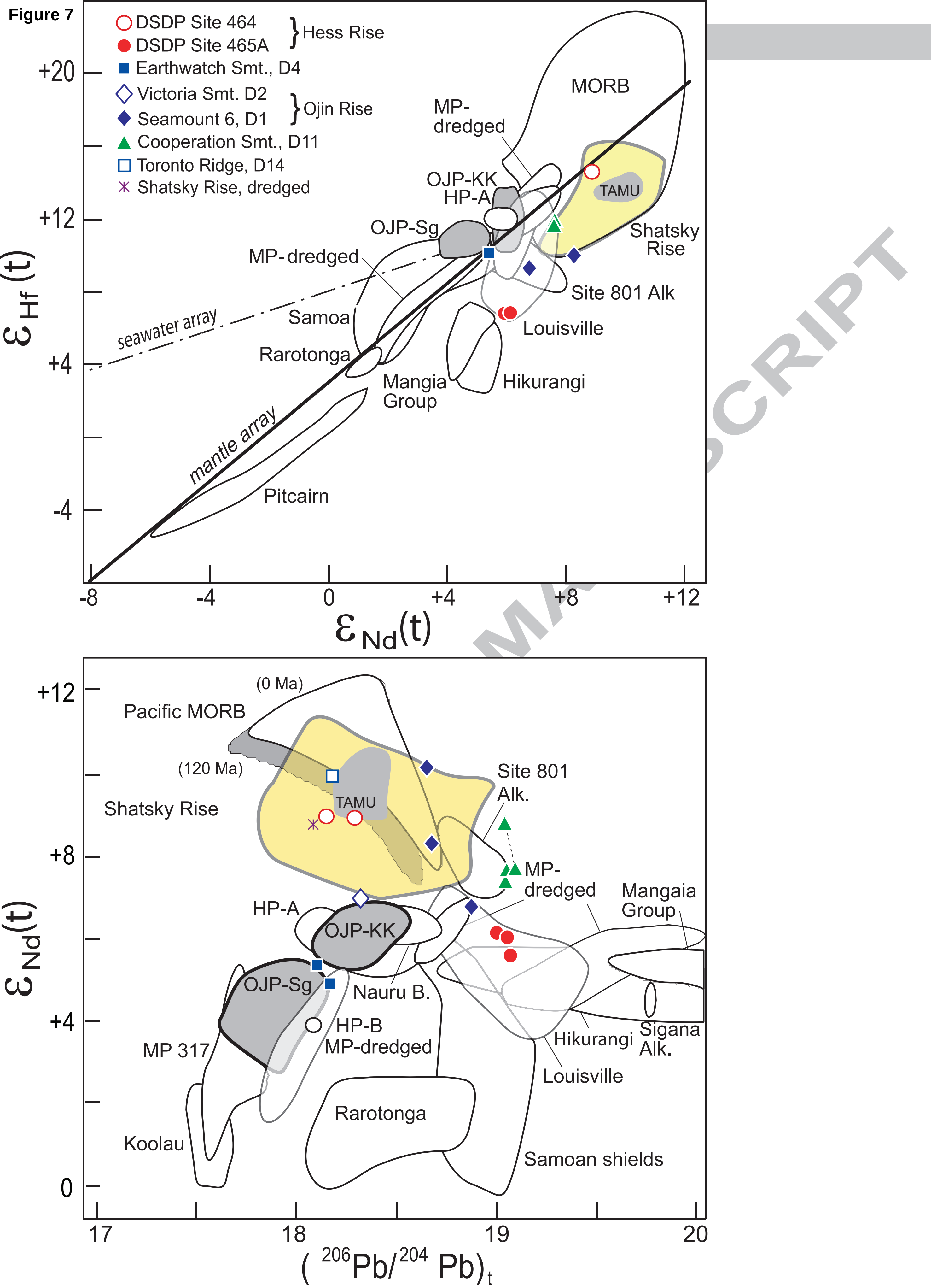

Figure 7

Figure 8

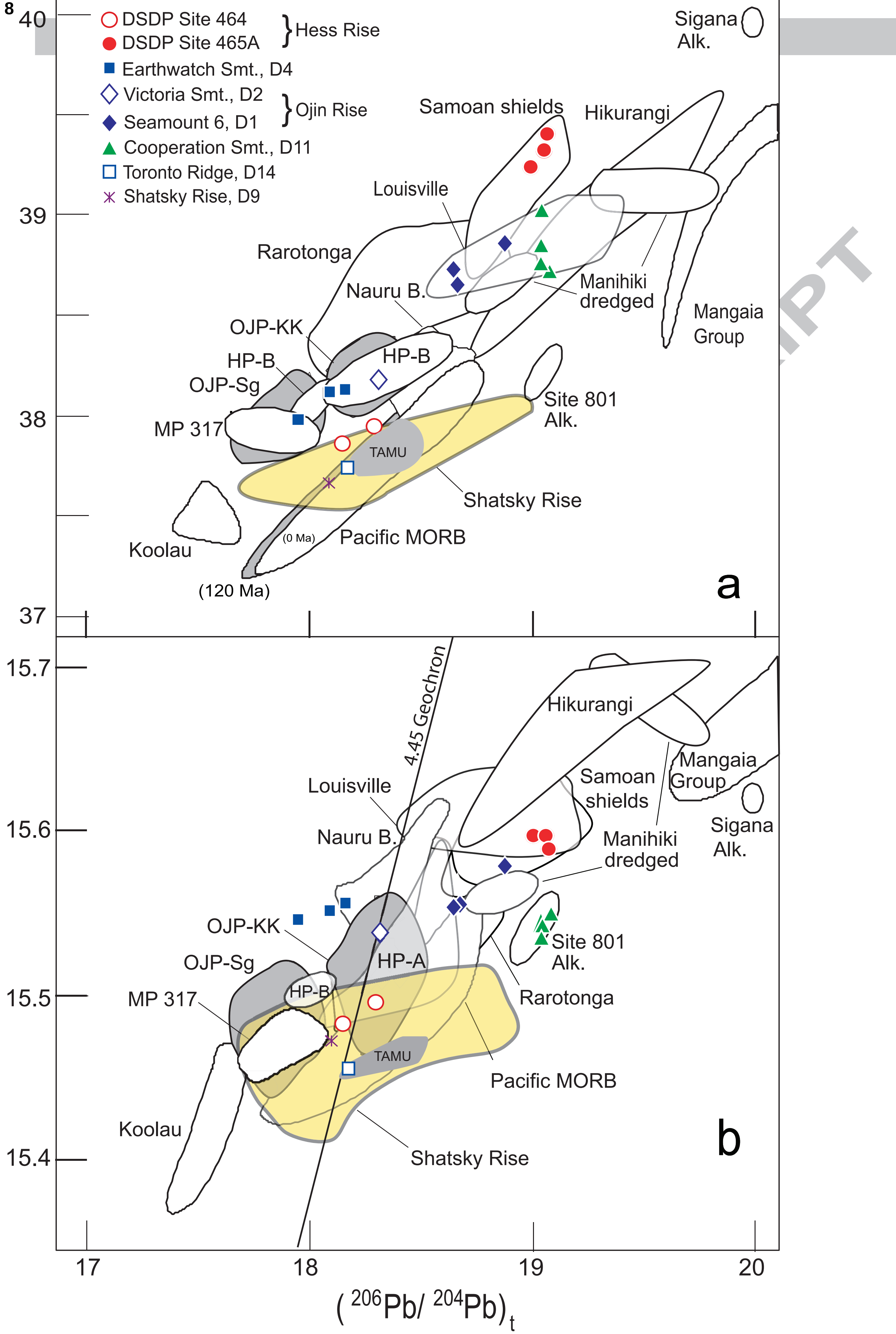

Figure 8

Figure 9

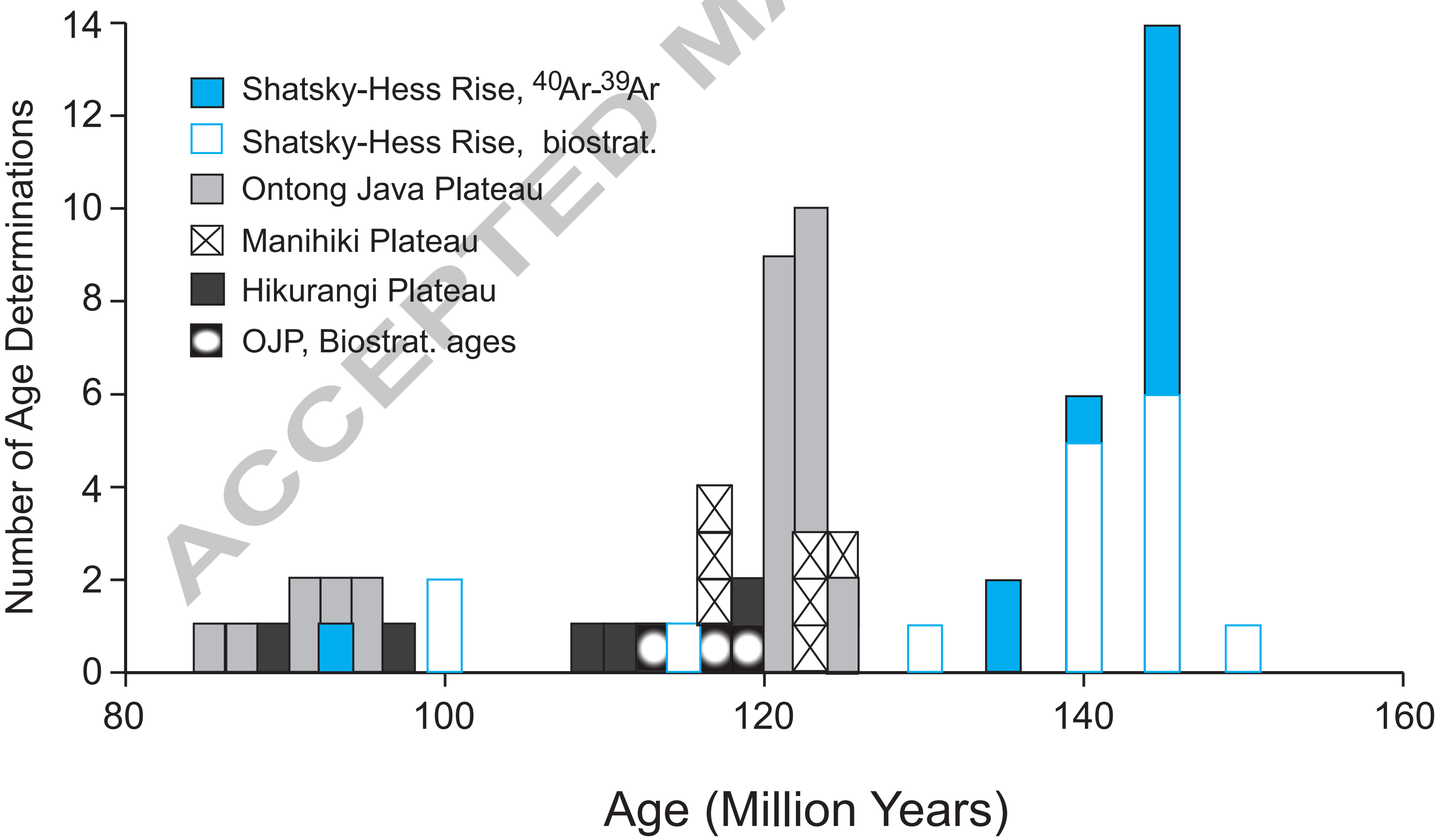

Figure 9

Figure 10

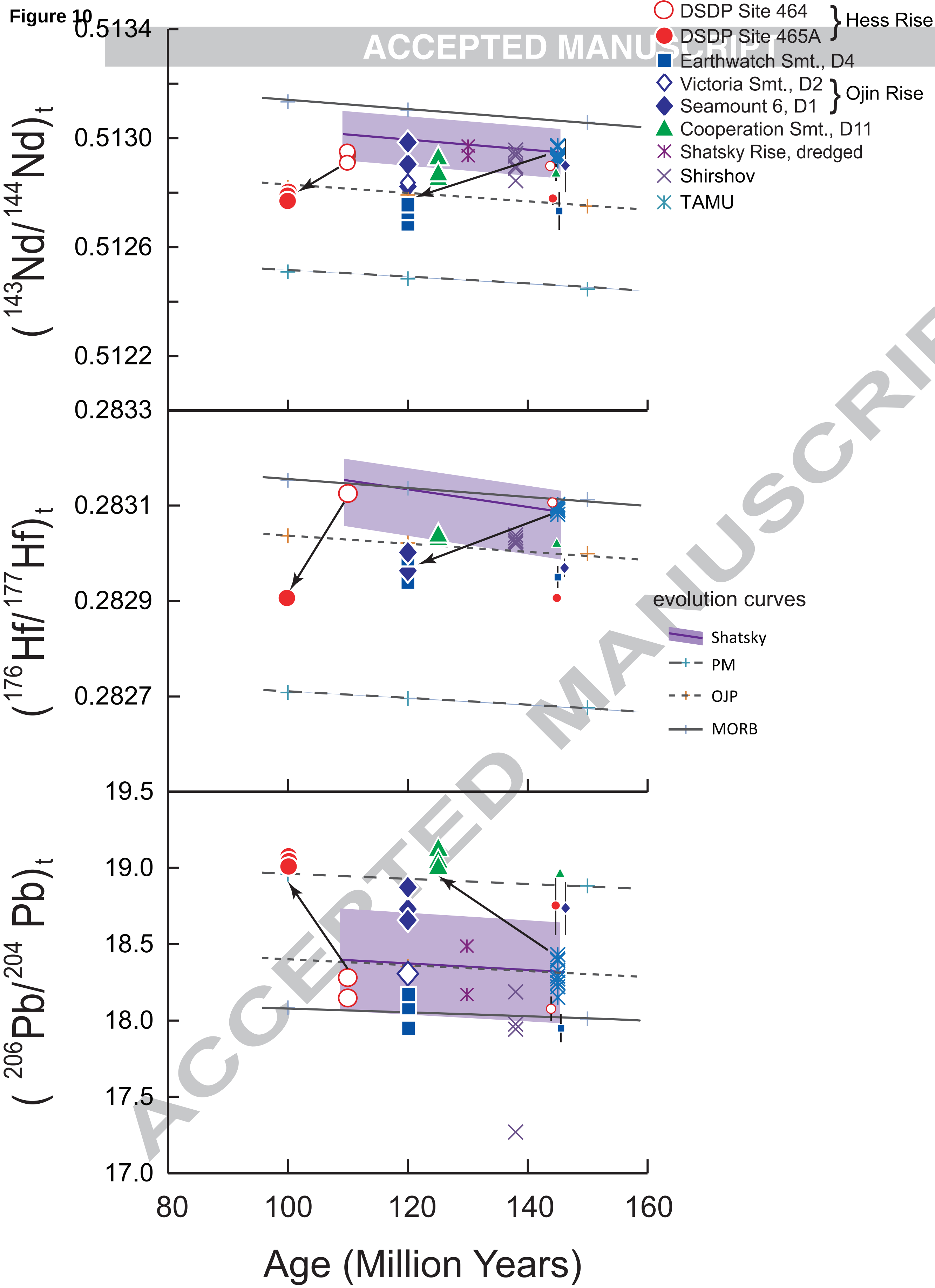

Figure 10